Neural correlates and determinants of approach-avoidance conflict in the prelimbic prefrontal cortex

Fernandez-Leon, J.A.[#1,2]; Engelke, D.S.[#1]; Aquino-Miranda, G.[#1]; Goodson, A.[3]; Do-Monte, F.H.[1,3]*.

[1] Dept. of Neurobiology & Anatomy, The University of Texas Health Science Center, Houston, TX77030, USA;

[2] Current Address: Exact Sciences Faculty, INTIA (UNCPBA-CICPBA) and CIFICEN (UNCPBA-CONICET-CICPBA), Tandil 7000, Buenos Aires, Argentina;

[3] Rice University, Houston, TX77030, USA

[#] These authors contributed equally to this work

*Corresponding author:

Fabricio H. Do Monte, DVM, PhD.
Department of Neurobiology and Anatomy, McGovern Medical School,
The University of Texas Health Science Center at Houston
6431 Fannin Street, Room 7.166, Houston, Texas 77030
Phone: 713-500-5613
Email: fabricio.h.domonte@uth.tmc.edu

Keywords: Prelimbic prefrontal cortex, electrophysiology, optogenetics, fear, reward, decision-making.

ABSTRACT

The recollection of environmental cues associated with threat or reward allows animals to select the most appropriate behavioral responses. Neurons in the prelimbic cortex (PL) respond to both threat- and reward-associated cues. However, it remains unknown whether PL regulates threat-avoidance vs. reward-approaching responses when an animals' decision depends on previously associated memories. Using a conflict model in which rats retrieve memories of shock- and food-paired cues, we observed two distinct phenotypes during conflict: i) rats that continued to press a lever for food (*Pressers*); and ii) rats that exhibited a complete suppression in food seeking (*Non-Pressers*). Single-unit recordings revealed that increased risk-taking behavior in *Pressers* is associated with persistent food-cue responses in PL, and reduced spontaneous activity in PL glutamatergic (PL^{GLUT}) neurons during conflict. Activating PL^{GLUT} neurons in *Pressers* attenuated food-seeking responses in a neutral context, whereas inhibiting PL^{GLUT} neurons in *Non-Pressers* reduced defensive responses and increased food approaching during conflict. Our results establish a causal role for PL^{GLUT} neurons in mediating individual variability in memory-based risky decision making by regulating threat-avoidance vs. reward-approach behaviors.

INTRODUCTION

The brain's ability to identify and discriminate cues associated with threat or reward allows organisms to respond appropriately to changes in the environment (Schultz, 2015; Hu, 2016). Animals respond to threatening cues with a series of defensive behaviors including avoidance responses that decrease their chances of being exposed to aversive outcomes (McNaughton and Corr, 2014; Krypotos et al., 2015; Cain, 2019). In contrast, reward cues have attractive and motivational properties that elicit approach behavior (Robinson and Flagel, 2009; Morales and Berridge, 2020). When animals are exposed to threat and reward cues simultaneously, an approach-avoidance conflict emerges, and decision-making processes are recruited to resolve the situation (Kirlic et al., 2017; Barker et al., 2019). While many studies have investigated the neural mechanisms that control threat-avoidance and reward-approach independently of each other, it is unclear how the brain uses previously learned information to regulate the opposing behavioral drives of avoiding threats and seeking rewards during a conflict situation.

Neurons in the prelimbic (PL) subregion of the medial prefrontal cortex (mPFC) change their firing rates in response to cues that predict either threat or reward (Baeg et al., 2001; Burgos-Robles et al., 2009; Burgos-Robles et al., 2013; Moorman and Aston-Jones, 2015; Dejean et al., 2016; Otis et al., 2017). Accordingly, activity in PL neurons is necessary for the retrieval of both food- and threat-associated memories (Sierra-Mercado et al., 2011; Courtin et al., 2014; Sangha et al., 2014; Do-Monte et al., 2015; Otis et al., 2017). PL neurons are reciprocally connected with the basolateral nucleus of the amygdala (BLA) (McDonald, 1991; Vertes, 2004), a region implicated in the

92 detection of threats or rewards (Amir et al., 2015; Namburi et al., 2015; Beyeler et al.,
93 2016; Zhang et al., 2020). During a risky foraging task in rats, dynamic modifications in
94 the activity of PL and BLA neurons correlate with the detection of imminent threats and
95 the defensive readiness for action (Kim et al., 2018; Kyriazi et al., 2020). In addition,
96 during a modified Pavlovian cue discrimination task involving footshocks as punishment,
97 increased activity in the BLA-PL pathway is sufficient and necessary for the expression
98 of freezing responses (Burgos-Robles et al., 2017), , a passive form of defensive
99 behavior. Conversely, inhibitory signaling in PL neurons correlates with threat
100 avoidance (Diehl et al., 2018), an active form of defensive behavior. While these studies
101 suggest a potential role of PL during motivational conflict involving states of certainty
102 (i.e., imminent threats), it is unknown whether changes in PL activity underlie the
103 behavioral variability in approach-avoidance responses under states of uncertainty,
104 when decision depends entirely on the retrieval of associated memories. It is also
105 unclear whether PL activity is necessary to coordinate appropriate behavioral responses
106 during conflict, and if so, which sub-types of PL neurons govern the competing
107 demands of approaching rewards vs. avoiding potential threats.

108 To address these questions, we designed an approach-avoidance conflict test
109 that assess the ability of rats to remember cues previously associated with either food
110 or footshocks to make a behavioral decision. Using a combination of optogenetics and
111 single-unit recordings, we investigated rats' individual variability in reward seeking and
112 defensive responses during the conflict test and correlated their behaviors (e.g.
113 freezing, avoidance, risk-assessment) with the firing rate of photoidentified
114 glutamatergic and GABAergic neurons in PL. We then examined the role of PL neurons

115 in risky decision-making by optogenetically manipulating PL activity with high temporal
116 resolution and cell-type specificity during the conflict test.

117

118 **RESULTS**

119 **Rats show individual variability in reward-seeking and defensive responses**
120 **during the approach-avoidance conflict test.**

121 To investigate the motivational conflict between approaching rewards and avoiding
122 potential threats, we established a behavioral model in which rats need to balance food
123 seeking with conditioned defensive responses based on their memories of previously
124 acquired cues. Food-restricted rats (18 g of chow per day) were initially placed in an
125 operant box and trained to press a lever for sucrose in the presence of audiovisual cues
126 that signaled the availability of food. Each lever press during the audiovisual cue
127 presentation resulted in the delivery of a sucrose pellet into a nearby dish (see Methods
128 for details). When rats reached 50% of discrimination during cued food-seeking, they
129 began lever-pressing for sucrose preferentially during the audiovisual cues
130 (**Supplementary Fig. 1A-B**). During the habituation day, rats were placed in an odor
131 arena and familiarized with the food cues and the neutral odor amyl acetate (see
132 Methods for details). Next, to pair the odor cue with an aversive stimulus, rats were
133 exposed to an olfactory threat conditioning training (Day 1). Animals were placed in an
134 operant box (conditioning box; **Fig. 1A left**) previously connected to an olfactometer
135 and habituated to one odor presentation (amyl acetate, 30 s) without footshock,
136 followed by five odor presentations of the same odor that co-terminated with an

electrical footshock (0.7 mA, 1 s duration, 270-390 s inter-trial intervals, **Fig. 1A far-left**). Food cues (30 s duration) were presented during the inter-trail intervals to assess lever press suppression. Rats showed robust defensive responses during the threat conditioning training, as evidenced by an increase in freezing during the conditioned odor presentation (**Fig. 1B**), a decrease in lever presses (**Fig. 1C**), and an increase in the latency to press the lever (**Fig. 1D**) during the presentation of the food cues across trials. After rats have acquired the reward and threat associations, they were returned to the same odor arena in which they were previously habituated and exposed to a test session (Day 2) (**Fig 1A, right**). The test session consisted of three different phases: (i) a *Reward Phase*, in which only the audiovisual cues signaling the availability of food were presented; (ii) an *Odor Phase*, in which only the conditioned odor was presented, and a (iii) *Conflict phase*, in which both the food cues and the conditioned odor were presented simultaneously (**Fig 1A, far-right**).

During the reward phase, rats spent ~40% of the time in the food area and pressed the lever for food in ~95% of the food cue trials, without exhibiting significant defensive behaviors (**Fig. 1E-J**). Introduction of the shock-paired odor during the odor phase reduced the percentage of time rats spent in the food area to ~15%, and increased defensive behaviors characterized by heightened freezing, avoidance, and risk-assessment responses (**Fig. 1E-H**). These defensive behaviors were attenuated by the introduction of food cues during the conflict phase, as evidenced by a reduction in the percentage of time avoiding the threatening odor **(Fig. 1F)** and an increase in the percentage of time approaching the food area **(Fig. 1H)**. This indicates that the concomitant presentation of food cues and shock-paired odor induced a behavioral

conflict in the animals. Interestingly, when we analyzed the percentage of rewarded presses during the conflict phase **(Fig. 1J)**, two behavioral phenotypes emerged: *i)* rats that continued to press the lever for food in the presence of the threatening odor (*Pressers,* **Fig. 1K**); and *ii)* rats that showed a complete suppression in lever presses in the presence of the threatening odor (*Non-Pressers*, **Fig. 1L**). We then separated the animals into two different groups and compared their behaviors during the entire test session **(Fig. 1K-R, Supplementary Movie 1)**. While *Pressers* and *Non-Pressers* showed similar behavioral responses during the reward phase (all p values > 0.05), *Pressers* showed a lower percentage of time exhibiting freezing and avoidance responses **(Fig. 1M,N)**, and a greater percentage of time approaching the food area **(Fig. 1P)** when compared to *Non-Pressers* during both the odor and the conflict phases. These individual phenotypes were not due to prior behavioral differences between the two groups because *Pressers* and *Non-Pressers* showed similar lever pressing rates during the cued food-seeking training, as well as the same levels of freezing, velocity (i.e., maximum speed), and lever presses during the threat conditioning phase (**Supplementary Fig. 1A-E**), indicating that increased risk-taking behavior in *Pressers* was not caused by prior differences in reward-seeking motivation. Together, our results demonstrate that our conflict model is a suitable paradigm to investigate the interactions between reward- and threat-associated memories. Given that rats exhibit individual differences in food seeking and defensive responses during the test session, we next took advantage of the two observed phenotypes to examine the neuronal correlates of risk-taking (*Pressers*) and risk-avoiding (*Non-Pressers*) behaviors in PL neurons.

PL neurons respond differently to reward cues in *Pressers* vs. *Non-Pressers* during conflict.

To investigate the role of PL neurons in regulating food-approach and threat-avoidance responses, we performed single-unit recordings across the different phases of the conflict test **(Fig. 2A)**. We aligned the activity of PL neurons to the onset of the food cues during the reward phase and tracked the firing rates of the same cells during the conflict phase. Using the behavioral classification shown in **Fig. 1J**, we separated the animals into *Pressers* or *Non-pressers* and compared changes in PL activity in response to food cues during the reward and conflict phases **(Fig. 2B-V)**. When PL activity was time-locked to the onset of the food cues during the reward phase, *Pressers* showed a higher number of food-cue responsive neurons than *Non-Pressers* **(Fig. 2C-D vs. Fig. 2M-N)**, with the proportion of excitatory and inhibitory responses being similar between the two groups. During the conflict phase, both *Pressers* and *Non-Pressers* showed a significant reduction in the number of food-cue responsive neurons (**Fig. 2C-D vs. 2M-N**), suggesting that PL neurons can distinguish between reward and conflict situations. However, *Pressers* exhibited persistent excitatory food cue responses **(Fig. 2E vs. Fig. 2O)**, which were higher in magnitude than in *Non-Pressers* **(Fig. 2F vs. Fig. 2P).** In addition, *Pressers* showed a higher magnitude of inhibitory food-cue responses during the reward phase and, in contrast to *Non-Pressers*, such responses were attenuated during the conflict phase **(Fig. 2FI-J vs. Fig. 2S-T).**

Next, we time-locked the activity of PL neurons to the onset of the food cues during the conflict phase. We observed a larger number of food-cue responsive neurons in *Pressers* compared to *Non-Pressers* **(Supplementary Fig. 2A-B vs. Supplementary**

Fig. 2K-L). Moreover, *Pressers* showed a higher magnitude of excitatory food cue responses during the conflict phase compared to *Non-Pressers* **(Supplementary Fig. 2C-F vs. Supplementary Fig. 2M-P)**, while the magnitude of the inhibitory food cue responses in *Pressers* were higher during the conflict phase compared to the reward phase **(Supplementary Fig. 2G-J vs. Supplementary Fig. 2Q-T)**.

To further explore whether changes in activity dynamics of PL neurons differ between *Pressers* and *Non-Pressers*, we compared the spontaneous firing rate of the neurons before vs. after each phase of the test session **(Supplementary Fig. 3A)**. While *Pressers* showed the same proportion of excitation and inhibition across the different phases, *Non-Pressers* exhibited a significant increase in the proportion of excitation during the conflict phase **(Supplementary Fig. 3B)**. This suggests that increased spontaneous activity in PL neurons during the conflict phase may be associated with the complete suppression in lever presses observed in *Non-Pressers* **(Fig. 1J)**. Collectively, these results suggest that differences in the number and magnitude of excitatory food cue responses, as well as in the spontaneous activity of PL neurons, during the conflict phase may contribute to the individual differences in risky decision-making observed between the two behavioral phenotypes.

Different subsets of PL neurons signal freezing, avoidance, and risk-assessment behaviors in both *Pressers* and *Non-pressers*.

To investigate whether PL activity correlates with the expression of distinct defensive behaviors during the test session, we used a pose estimation algorithm (Deep Lab Cut, see Methods for details) to identify the onset of freezing, avoidance or risk-assessment

229 responses and align these time points with the activity of PL neurons. We found that a
230 small percentage of PL neurons changed their firing rates during the onset of freezing
231 (**Fig. 3A**), avoidance (**Fig. 3B**), or risk-assessment (**Fig. 3C**) behaviors in both *Pressers*
232 and *Non-Pressers*, with a similar proportion of excitatory and inhibitory responses being
233 observed in the two groups **(Fig. 3A-I)**. Interestingly, most PL responsive neurons
234 (80%) changed their activities exclusively during the onset of one of these three
235 behaviors, with avoidance-responsive cells also responding during the onset of risk-
236 assessment behavior **(Fig. 3J-M)**. These results suggest that different subsets of PL
237 neurons signal distinct behavioral outcomes during a conflict situation, with only a
238 reduced number of PL neurons encoding the aversive salience of environmental cues
239 independently of the behavioral defensive response expressed by the animal.
240

241 ***Pressers* and *Non-Pressers* show significant differences in delta and theta**
242 **oscillations in PL**

243 Previous studies have shown that oscillations in mPFC neuronal activity at
244 different frequency bands correlate with distinct behavioral states in both rodents and
245 humans (Narayanan et al., 2013; Harris and Gordon, 2015). Neural oscillations in the
246 mPFC emerge from the network of excitatory and inhibitory synaptic connections and
247 are thought to contribute to neural communication when subjects engage in reward and
248 threat memory tasks (Hyman et al., 2011; Likhtik and Paz, 2015; Park and Moghaddam,
249 2017; Widge et al., 2019). To investigate whether *Pressers* and *Non-Pressers* show
250 significant differences in PL oscillations during conflict, we recorded local field potentials
251 (LFPs) from PL neurons and calculated the average of power spectral density (PSD) at

252 different frequencies across the test session. After comparing the PSD contribution for
253 each frequency range in *Pressers* and *Non-Pressers,* we observed that most of the
254 signal was prevenient from the delta (0-4 Hz) and theta (4-10 Hz) bands, with a much
255 smaller contribution coming from the alpha (10-14 Hz), beta (14-35 Hz), and gamma
256 (>35 Hz) frequencies **(Fig. 4A)**. We therefore focused our analyses on these two bands
257 and found that *Pressers* displayed increased power in the delta band, whereas *Non-*
258 *Pressers* exhibited increased power in the theta band during the three phases of the
259 test session **(Fig. 4B-C)**. Differences between *Pressers* and *Non-Pressers* were also
260 observed in the time-frequency domain through changes in the log of PSD for delta and
261 theta bands across the different phases **(Fig. 4D-E)**. These results indicate that
262 phenotypic differences in approach-avoidance conflict are associated with distinct
263 oscillatory frequencies in PL.
264

265 **In pressers, PL^{GLUT} neurons show reduced spontaneous activity during the**
266 **conflict phase.**

267 The rodent mPFC, including PL, is primarily composed of excitatory
268 glutamatergic cells that correspond to 75-85% of the neurons in this area. In contrast,
269 inhibitory GABAergic interneurons comprise 15-25% of the local neurons (Santana et
270 al., 2004; Gabbott et al., 2005). Previous studies have shown that PL glutamatergic
271 (PL^{GLUT}) neurons are necessary for the retrieval of conditioned threat responses (Do-
272 Monte et al., 2015), whereas PL GABAergic (PL^{GABA}) neurons are implicated in both the
273 encoding and the retrieval of threat associations by regulating the firing rate of PL^{GLUT}
274 neurons (Courtin et al., 2014; Cummings and Clem, 2020). In addition, during foraging

275 in a safe context, food-associated cues activate both PL^{GLUT} and PL^{GABA} neurons
276 (Burgos-Robles et al., 2013; Gaykema et al., 2014), and inactivation of PL^{GLUT} neurons
277 may increase or reduce conditioned food-seeking responses depending on the specific
278 downstream projections that are being modulated (Otis et al., 2017). While these
279 studies suggest a role for both PL^{GLUT} and PL^{GABA} neurons in the regulation of threat
280 and food-seeking responses in isolation, it remains unexplored how these two subsets
281 of PL neurons regulate the trade-off between seeking rewards and avoiding potential
282 threats during a conflict situation. To address this question, we combined single-unit
283 recordings with optogenetics to track the neuronal activity of photoidentified PL^{GLUT} and
284 PL^{GABA} neurons during the test session.

285 For photoidentification of PL^{GLUT} neurons, we injected into PL a viral vector (AAV-
286 CaMKIIα-hChR2-(H134R)-eYFP) with a gene promoter (CaMKIIα) that favors the
287 expression of the light-activated cation channel channelrhodopsin (ChR2) in PL^{GLUT}
288 neurons. This CaMKIIα labeling approach has been successfully used in previous
289 studies (Gradinaru et al., 2009; Tye et al., 2011) and was validated here for PL neurons
290 by showing a lack of immunocolabeling between the viral vector and the GABAergic
291 marker GAD67 **(Fig. 5A)**. Rats expressing ChR2 selectively in PL^{GLUT} neurons were
292 implanted with an optrode into the same region for optogenetic-mediated identification
293 of PL^{GLUT} neurons at the end of the behavioral session **(Fig. 5B)**. Among the recorded
294 PL cells, 39 out of 104 neurons (n = 5 rats) showed short-latency responses (< 6 ms) to
295 laser illumination and were classified as PL^{GLUT} neurons **(Fig. 5C-D** and Methods**)**.
296 Previous studies have shown that photoactivation of PL^{GLUT} neurons can lead to indirect
297 activation of synaptically connected neurons in the region, but these indirect responses

298 to laser illumination in cortical regions take longer than 9 ms to occur (Lima et al., 2009).
299 For photoidentification of PL^{GABA} neurons, we injected into PL a viral vector (AAV-mDlx-
300 ChR2-mCherry) with a gene promoter (mDlx) that favors the expression of ChR2 in
301 PL^{GABA} neurons. This mDlx labeling approach has been successfully used in previous
302 studies (Dimidschstein et al., 2016; Sun et al., 2020), and was validated here for PL
303 neurons by using two different methods: an immunohistochemical approach that
304 resulted in significant immunocolabeling between the viral vector and the GABAergic
305 marker GAD67 **(Fig. 5E)**, and an *in situ* hybridization approach which confirmed that
306 ~88% of the cells labeled with the viral vector also expressed the GABAergic marker
307 vGAT **(Supplementary Fig. 4A-B)**. Rats expressing ChR2 selectively in PL^{GABA}
308 neurons were implanted with an optrode into the same region for optogenetic-mediated
309 identification of PL^{GABA} neurons at the end of the behavioral session **(Fig. 5F)**. Among
310 the recorded PL cells, 84 out of 338 neurons (n = 19 rats) showed short-latency
311 responses to laser illumination (< 12 ms) and were classified as PL^{GABA} neurons **(Fig.
312 5G-H and Methods)**. A longer latency criterion was used for GABAergic neurons
313 because indirect photoactivation of neighboring cells would require a disinhibitory
314 mechanism that has been shown to take longer than 15 ms in cortical regions (Pi et al.,
315 2013).
316 After separating the photoidentified cells into PL^{GLUT} and PL^{GABA} neurons, we
317 aligned their activities to the onset of the food cues and compared changes in firing
318 rates from the reward to the conflict phase in *Pressers* **(Fig. 5I)**. We observed that the
319 proportions of excitatory and inhibitory food cue responses for PL^{GLUT} and PL^{GABA}
320 neurons were similar during the reward and the conflict phases **(Fig. 5J-K)**. Next, we

321 analyzed the spontaneous activity of PL^{GLUT} and PL^{GABA} neurons and compared
322 changes in their firing rates across the different phases of the test session **(Fig. 5L)**. We
323 found that the average firing rate of PL^{GLUT} neurons remained the same across the
324 different phases of the test (~5 Hz; **Fig. 5M**), with most of the cells (53%) changing their
325 activities in more than one session **(Fig. 5N)**. A group analysis of the firing rates across
326 phases demonstrated that PL^{GLUT} neurons were disinhibited during the odor phase, and
327 subsequently inhibited during the conflict phase when *Pressers* resumed searching for
328 food **(Fig. 5O)**. Similar to PL^{GLUT} neurons, the average firing rate of PL^{GABA} neurons also
329 remained the same across the different phases of the test (~8 Hz, **Fig. 5P)**, with most of
330 the cells (65%) changing their activities in more than one session **(Fig. 5Q)**. However, in
331 contrast to PL^{GLUT} neurons, a group analysis of the firing rates of PL^{GABA} neurons did
332 not reveal significant differences across the phases **(Fig. 5R)**. Because PL is comprised
333 of different subpopulations of interneurons that inhibit each other during food seeking or
334 defensive responses (Gaykema et al., 2014; Cummings and Clem, 2020), we cannot
335 rule out the possibility that distinct subsets of PL^{GABA} neurons were preferentially
336 recruited during each one of the phases.

337 To evaluate how the spontaneous activity of the same PL neurons changed
338 during the test session, we tracked the firing rate of PL^{GLUT} and PL^{GABA} neurons across
339 the different phases. We found that all PL^{GLUT} neurons that were either excited or
340 inhibited during the reward phase responded in opposite direction or did not change
341 their activities during the odor phase **(Supplementary Figure 5A-B)**, suggesting the
342 existence of distinct subpopulations of PL^{GLUT} neurons that encode valence-specific
343 information. In contrast, no significant differences in the proportions of excitation and

344 inhibition were observed in PL^{GABA} neurons during the transition from reward to odor
345 phase nor during the transition from odor to conflict phase for both subsets of PL
346 neurons **(Supplementary Figure 5C-F)**. Furthermore, both PL^{GLUT} and PL^{GABA} neurons
347 showed the same proportion of excitatory and inhibitory responses during the onset of
348 freezing, avoidance, or risk-assessment behaviors **(Supplementary Figure 6A-C)**,
349 indicating that both subsets of PL neurons may contribute to the expression of distinct
350 defensive responses during conflict. Together, our data suggest that PL^{GLUT} neurons
351 are disinhibited when foraging rats exhibit increased defensive behaviors in response to
352 the conditioned odor and become inhibited again when animals resume searching for
353 food during the conflict phase.
354

355 **Putative classification of PL neurons based on spike waveform and spike timing**
356 **parameters is insufficient to differentiate glutamatergic and GABAergic cells**

357 Previous single-unit recording studies have used an indirect cluster analysis of
358 spike waveform and spike timing parameters to classify neurons into putative
359 glutamatergic or putative GABAergic cells (Hassani et al., 2009; Courtin et al., 2014;
360 Fan et al., 2017). While it is widely accepted that glutamatergic neurons exhibit longer
361 spike duration and lower firing rate than GABAergic neurons (Mruczek and Sheinberg,
362 2012; Ono et al., 2017), a direct comparison between optogenetic photoidentification
363 and putative classification of PL neurons *in vivo* is currently missing to confirm that
364 extracellular spike parameters can be reliably used to separate glutamatergic and
365 GABAergic cells.

366 We sought to address this question by extracting the extracellular spiking
367 properties of the 123 photoidentified PL neurons shown in **Figure 5** and plotting their
368 values to perform a cluster analysis separation. Because the amplitude of the waveform
369 has been shown to directly correlate with the distance between the recording electrode
370 and the neuronal soma (Weir et al., 2014), we limited our analyses to the duration of the
371 action potentials (i.e., spike half-width) and the firing rate of the neurons (i.e.,
372 frequency), similar to previous putative classifications *in vivo* (Frank et al., 2001;
373 Constantinidis and Goldman-Rakic, 2002; Bartho et al., 2004). Using an unbiased
374 unsupervised cluster-separation algorithm, we separated the cells into putative PL^{GLUT}
375 and putative PL^{GABA} neurons based on spike waveform and spike timing features by
376 using k-means++ algorithm as a heuristic to find centroid seeds for k-means clustering
377 (see Methods for details). Only *in vivo* photoidentified GABAergic or glutamatergic
378 neurons were considered for this analysis. The spike half-width feature was the driving
379 force for the classification and indicated a division of clusters at ~0.175 ms
380 **(Supplementary Figure 7A)**. By marking the cells that were previously photoidentified
381 as PL^{GLUT} or PL^{GABA} neurons on the same cluster distribution, we calculated the
382 percentage of PL^{GLUT} or PL^{GABA} neurons that were correctly identified with the putative
383 classification **(Supplementary Figure 7A-B)**. Surprisingly, we observed less than 40%
384 of overlapping between the optogenetic photoidentification and the putative analysis
385 **(Supplementary Figure 7B-C)**, indicating that cell-type putative classification of
386 glutamatergic and GABAergic neurons in PL should be treated with caution. These
387 results are consistent with prior studies *in vivo* showing that pyramidal and inhibitory
388 neurons exhibit a wide variety of frequencies and spike durations, which alone may not

389 be sufficient for putative cell-type classification (Vigneswaran et al., 2011; Becchetti et
390 al., 2012; Weir et al., 2014).
391
392 **Photoactivation of PL^{GLUT}, but not PL^{GABA} neurons, suppresses reward-seeking**
393 **responses.**
394 To further establish whether changes in the activity of PL neurons can alter cue-
395 triggered food-seeking responses, we used an optogenetic approach to selectively
396 activate either PL^{GLUT} or PL^{GABA} neurons during a cued food-seeking test in a neutral
397 context. We initially infused either the viral vector AAV-CaMKIIα-ChR2-eYFP **(Fig. 6A)**
398 or AAV-mDlx-ChR2-mCherry **(Fig. 6E)** into PL and implanted an optrode into the same
399 region to examine how photoactivation of PL^{GLUT} or PL^{GABA} neurons change local
400 activity. Laser illumination of PL^{GLUT} somata increased the firing rate of most responsive
401 PL neurons (9 out of 20 neurons, 45%), with some neurons showing reduced activity (6
402 out of 20 neurons, 30%, **Fig. 6B-D**). Neurons that increased their activities showed
403 shorter response latencies (2.1 ±0.24 s) compared to neurons that reduced their
404 activities (41.3 ± 5.57 s), suggesting direct responses (i.e., opsin-mediated) versus
405 indirect responses (i.e., multi-synaptic), respectively. Conversely, laser illumination of
406 PL^{GABA} somata reduced the firing rate of all responsive PL neurons (16 out of 22
407 neurons, 73%; **Fig. 6F-H)**, indicating a suppression in local activity. After investigating
408 the local effects of photoactivating either PL^{GLUT} and PL^{GABA} neurons, we infused
409 another set of animals with the same viral vectors in PL and implanted bilateral optical
410 fibers into the same region to manipulate PL activity during the cued food-seeking test
411 **(Fig. 6I-J)**. Rats expressing only eYFP in PL were used to control for any nonspecific

412 effects of viral transduction or laser heating. To assess the effects of PL photoactivation
413 on lever presses, we alternated two trials of food cues with the laser on vs. laser off
414 conditions **(Fig. 6K-L)**. Photoactivation of PL^{GLUT} (CaMKIIα-ChR2), but not PL^{GABA}
415 (mDlx-ChR2) neurons, reduced the frequency of lever presses **(Fig. 6M)** and increased
416 the latency for the first press after the cue onset **(Fig. 6N)**, when compared to control
417 group. Photoactivation of either PL^{GLUT} or PL^{GABA} neurons did not induce freezing
418 behavior **(Fig. 6O)**. These results are consistent with our electrophysiological recordings
419 in **Fig. 5O** showing that increased inhibition in the firing rate of PL^{GLUT} neurons
420 correlates with augmented reward-seeking responses during conflict. Overall, these
421 findings suggest that increasing the activity of PL^{GLUT} neurons is sufficient to suppress
422 cued reward-seeking responses in a neutral context.
423

424 **Photoinhibition of PL^{GLUT} neurons in *Non-pressers* reduces freezing responses**
425 **and increases food approaching during conflict.**

426 Our electrophysiological experiments in **Fig. 5O** demonstrate that PL^{GLUT} neurons are
427 disinhibited when rats express defensive responses to the conditioned odor. In addition,
428 our photoactivation experiments in **Fig. 6K-O** indicate that increasing the activity of
429 PL^{GLUT} neurons suppresses cued reward-seeking behavior in rats that are pressing a
430 lever for food. We next hypothesized that photoinhibition PL^{GLUT} neurons during conflict
431 would attenuate defensive behaviors and rescue food-seeking responses in *Non-*
432 *Pressers*. To test this hypothesis, we injected a group of rats with the viral vector AAV-
433 CaMKIIα-eNpHR-eYFP (or AAV-CaMKIIα-eYFP) into PL to express the inhibitory opsin
434 halorhodopsin (or eYFP control) selectively in PL^{GLUT} neurons **(Fig. 7A)**. Rats were

435 initially exposed to a cued food-seeking test to assess the effects of photoinhibition of
436 PL^{GLUT} neurons on food-seeking responses in a neutral context. We observed that
437 photoinhibition of PL^{GLUT} neurons had no effect on lever pressing rate, latency to press
438 the lever or freezing responses before threat conditioning **(Supplementary Fig. 8A-E)**.
439 Animals were then threat conditioned as in **Fig. 1** and on the following day exposed to
440 the odor arena for a test session. During the conflict phase, the first pair of food cues
441 was used to classify the animals into *Pressers* and *Non-Pressers*, whereas the
442 subsequent pairs of food cues were alternated between laser on and laser off conditions
443 to assess the effects of illumination of PL^{GLUT} neurons on approach-avoidance
444 responses **(Fig. 7B-C)**. Remarkably, photoinhibition of PL^{GLUT} neurons (CaMKIIα-
445 eNpHR) in *Non-Pressers* reduced the percentage of time rats spent freezing **(Fig. 7D)**
446 and avoiding the odor area **(Fig. 7E)**, and increased the percentage of time rats spent
447 approaching the food area **(Fig 7F)** during the food cue presentation, when compared to
448 the eYFP-control group. Despite the increase in food approaching behavior,
449 photoinhibition of the same cells had no effects on lever pressing responses **(Fig. 7G-**
450 **H)**. In another subset of *Non-Presser* rats, photoactivation of PL^{GABA} neurons (mDlx-
451 ChR2) did not alter food seeking nor defensive responses during the conflict phase,
452 when compared to the mCherry-control group **(Fig 7I-P)**. Taken together, these results
453 demonstrate that reduced activity in PL^{GLUT} neurons during conflict situations reduces
454 defensive responses and biases rats' behavior toward food seeking.

455

456

457

DISCUSSION

Using a novel approach-avoidance conflict test, we demonstrated that PL neurons regulate reward-approach vs. threat-avoidance responses during situations of uncertainty, when rats use previously associated memories to guide their decisions. We found that increased risk-taking behavior in *Pressers* was associated with a larger number of food-cue responses in PL neurons, which were higher in magnitude and persisted during the conflict phase, when compared to *Non-Pressers*. In addition, PL^{GLUT} neurons showed reduced spontaneous activity during risky reward seeking and photoactivation of these cells in a neutral context was sufficient to suppress lever press responses. Accordingly, photoinhibition of PL^{GLUT} neurons at the onset of the food cues in *Non-Pressers* reduced defensive responses and increased food-approaching during the conflict phase, consistent with our observation that a small fraction of PL neurons changed their activity at the onset of freezing, avoidance or risk-assessment responses. Altogether, these results suggest that under memory-based conflict situations, reduced or increased activity in PL^{GLUT} neurons can favor the behavioral expression of food-approaching or threat-avoidance responses, respectively.

During our approach-avoidance conflict test, *Pressers* and *Non-Pressers* showed similar levels of lever pressing before the conflict phase (e.g., cued food-seeking training, threat conditioning, and reward phases). This observation suggests that these two individual phenotypes most likely emerged during the test session and were independent of prior differences in sucrose preference or food-seeking motivation. Similarly, because both groups exhibited the same percentage of freezing during the olfactory threat conditioning session, the increased defensive behaviors and the

481 reduced food-seeking responses observed in *Non-Pressers* during the test session
482 were unlikely due to higher acquisition of conditioned threat responses. Furthermore,
483 other external factors such as shock sensitivity or pain tolerance cannot be accounted
484 for the individual differences observed in our experiments because both groups reacted
485 equally to the unconditioned stimulus (i.e., velocity measured as maximum speed after
486 the footshocks) and, different from other conflict tasks using footshocks as a
487 punishment during the conflict test (Geller, 1960; Vogel et al., 1971; Oberrauch et al.,
488 2019), in our model rats were not exposed to footshocks during the conflict phase.
489 Therefore, the most plausible interpretation for the behavioral differences observed in
490 our task is that *Pressers* and *Non-Pressers* have allocated distinct motivational
491 significance to the food- or shock-paired cues during the test session.

492 Individual differences in risky decision making have also been reported in other
493 studies using rodent models of behavioral conflict involving footshock punishment
494 (Simon et al., 2009; Jean-Richard-Dit-Bressel et al., 2019; Bravo-Rivera et al., 2021),
495 reversal learning (Bari et al., 2010), or variations in reward probability (Ainslie, 1975; St
496 Onge and Floresco, 2009; Dellu-Hagedorn et al., 2018), although the neural
497 mechanisms underlying such differences are less clear. Evidence indicates that some of
498 the neurobiological bases of individual variation in stimulus-reward response depend on
499 differences in dopamine levels in subcortical circuits (Tomie et al., 2000; Flagel et al.,
500 2007; Flagel et al., 2011), which are regulated by top-down mechanisms involving the
501 mPFC (Ferenczi et al., 2016; Haight et al., 2017; Serrano-Barroso et al., 2019).
502 Accordingly, our neural correlate analyses of risk-taking vs. risk-avoiding behaviors in
503 the PL subregion of the mPFC revealed some clear differences between the two

504 phenotypes, suggesting that PL neurons participate in behavioral selection when rats'
505 decision depends on the conflicting memories of reward and threat. One interesting
506 finding in our study was the observation that *Pressers* showed a larger number and a
507 higher magnitude of food-cue responses during the conflict phase when compared to
508 *Non-Pressers*, indicating that PL neurons can differentiate between situations involving
509 motivational conflict and those that do not. Because PL neurons are known for encoding
510 the value of reward-predictive cues (Sharpe and Killcross, 2015; Otis et al., 2017), the
511 increase in the number and magnitude of food cue responses observed in *Pressers*
512 might result in a greater allocation of attention to food cues, which would explain the
513 persistent reward-seeking responses observed in this group during motivational conflict.
514 In support of this interpretation, reward-paired cues can acquire motivational salience in
515 some subjects and become sufficient to elicit reward-seeking responses in both rodents
516 (Robinson and Flagel, 2009; Robinson et al., 2014) and humans (Smith et al., 2011;
517 Jensen and Walter, 2014). Consistently, *Pressers* also showed a larger number and a
518 higher magnitude of food cue responses in PL before the conflict phase (i.e., reward
519 phase), although the percentage of rewarded presses and the latency to press the lever
520 during the reward phase were similar between the two groups.

521 Another possible interpretation for the differences in food-cue responses in
522 *Pressers* and *Non-Pressers* is the reduced excitatory-food cue responses in *Non-*
523 *Pressers,* which may be mediated by cue-evoked inhibitory inputs to PL during the
524 conflict phase. While the source of this inhibition is unclear, a potential candidate are
525 GABAergic neurons in the ventral tegmental area (VTA^{GABA}), which correspond to 35%
526 of the cells in this region and send significant projections to PL (Nair-Roberts et al.,

527 2008; Breton et al., 2019). Previous studies have shown that VTA^{GABA} neurons change
528 their firing rates in response to reward-predicting cues (Cohen et al., 2012), and
529 chemogenetic activation of these cells suppress the activity of local dopaminergic
530 neurons (van Zessen et al., 2012), reduces cue-evoked sucrose-seeking responses
531 (Wakabayashi et al., 2019), and induces conditioned place aversion in rodents (Tan et
532 al., 2012). Future studies need to determine whether this regulation of rewarding and
533 aversive responses by VTA^{GABA} neurons can also be attributed to their long-range
534 inhibitory projections to PL neurons, particularly during conflict situations.

535 Differences in risk-taking and risk-avoiding behaviors were also reflected on LFP
536 frequencies in PL neurons in the beginning of the test session, with *Pressers* and *Non-*
537 *Pressers* displaying increased power in the delta or theta bands, respectively. These
538 findings are in corroboration with previous studies showing that increased delta power
539 activity in the mPFC is associated with both reward-seeking and preparatory attention
540 (Horst and Laubach, 2013; Totah et al., 2013; Emmons et al., 2016), whereas
541 augmented theta power in the mPFC or synchronized theta activity between mPFC and
542 BLA is correlated with the expression of avoidance responses or the consolidation of
543 threat memories, respectively (Popa et al., 2010; Padilla-Coreano et al., 2019). More
544 specifically, increased synchrony between mPFC and BLA activity in the theta
545 frequency range has been reported for animals that successfully differentiate between
546 aversive and safe cues (or environments) during a differential threat conditioning task
547 (or an open field arena) (Likhtik et al., 2014; Stujenske et al., 2014). In addition, prior
548 studies have shown that 4 Hz LFP oscillations in the mPFC and BLA were strongly
549 synchronized during conditioned freezing episodes (Courtin et al., 2014; Dejean et al.,

550 2016; Karalis et al., 2016), and these sustained 4 Hz oscillations in the mPFC were
551 independent of hippocampal low-theta oscillations, suggesting that they were internally
552 generated in the mPFC during the expression of freezing behavior (Karalis et al., 2016).
553 Consistent with these findings, in our study *Non-Pressers* showed increased theta
554 activity and marked 4 Hz oscillations in PL neurons, which were associated with better
555 discrimination between reward and threat cues and increased freezing responses
556 during the test session, when compared to *Pressers*.

557 Increased risk-taking behavior in *Pressers* was associated with a higher number
558 of PL^{GLUT} neurons showing reduced spontaneous activity during the conflict phase. In
559 contrast, risk-avoiding responses in *Non-Pressers* were associated with increased
560 spontaneous activity during conflict. While this set of results suggest that distinct
561 patterns of PL activity are associated with risk-taking or risk-avoiding behaviors in
562 conflict situations, our optogenetic manipulation provided a causal role for PL^{GLUT}
563 neurons in the regulation of approach-avoidance conflict. For instance, the reduction in
564 food-seeking responses during photoactivation of PL^{GLUT} neurons indicates that
565 increased activity in PL pyramidal cells is sufficient to recapitulate the reward-seeking
566 suppression observed during conflict. Our findings agree with previous studies showing
567 that increased activity in mPFC neurons, including PL, attenuates reward-seeking
568 responses in a neutral context (Berglind et al., 2007; Chen et al., 2013; Ferenczi et al.,
569 2016; but see: Warthen et al., 2016), an effect that has been attributed, at least in part,
570 to downstream projections to the paraventricular nucleus of the thalamus (PVT) (Otis et
571 al., 2017). Notably, PVT neurons are necessary for the retrieval of both reward- and
572 threat-associated memories (for a review see: Do Monte et al., 2016; Millan et al., 2017;

573 McGinty and Otis, 2020; Penzo and Gao, 2021), and activity in PVT neurons has
574 recently been shown to be associated with the regulation of approach-avoidance
575 responses during situations of conflict (Choi and McNally, 2017; Choi et al., 2019;
576 Engelke et al., 2021), suggesting a potential target by which PL glutamatergic neurons
577 may exert their effects.

578 Considering that *Pressers* showed a higher number of excitatory food-cue
579 responses than *Non-Pressers*, it is counterintuitive that photoactivation of PL^{GLUT}
580 neurons during the food cue onset resulted in reduced food-seeking responses.
581 However, it is important to note that our optogenetic manipulation not only altered the
582 activity of food-cue responsive neurons, but mostly the global activity of other PL^{GLUT}
583 neurons. Thus, it is possible that increased activity in the firing rate of PL^{GLUT} neurons
584 may result in reduced signal-to-noise ratio during the food cue onset (Kroener et al.,
585 2009; McGinley et al., 2015), and consequently decreased food-seeking responses. In
586 contrast, by reducing their spontaneous firing rates during conflict situations, PL^{GLUT}
587 neurons become more likely to fire in response to food cues due to an increase in the
588 signal-to-noise ratio, thereby resulting in persistent reward-seeking responses during
589 the conflict phase as we propose in our schematic in Fig. 8.

590 Additionally, our findings showing that inactivation of PL^{GLUT} neurons increases
591 food-approaching responses in *Non-Pressers* suggest that PL activity is indispensable
592 to inhibit reward pursuit in the presence of threat-associated cues. The lack of effects on
593 lever pressing may indicate that other parallel brain regions may be modulating the
594 suppression of operant lever-press responses during conflict. Alternatively,
595 photoinhibition of PL^{GLUT} neurons was not large enough to produce a more global effect

596 on risky behavior (i.e., completely restore lever presses). Collectively, these results add
597 to a growing literature indicating that PL neurons are necessary to guide appropriate
598 food-seeking behavior in tasks that rely on discrimination among environmental cues
599 (Marquis et al., 2007; Sangha et al., 2014; Moorman and Aston-Jones, 2015) or
600 decision-making tasks involving risk of punishment in which animals need to: i) adapt
601 choice behavior during shifts in risk contingencies (Orsini et al., 2018), ii) regulate
602 behavioral flexibility (Radke et al., 2015; Capuzzo and Floresco, 2020), or iii) suppress
603 reward seeking in response to conditioned aversive stimuli (Kim et al., 2017; Piantadosi
604 et al., 2020). Moreover, our results are in accordance with previous findings
605 demonstrating that inactivation of PL neurons, or their inputs from BLA, increases risk-
606 taking behavior in a conflict task in which rats needed to refrain from consuming
607 sucrose to avoid a footshock (Burgos-Robles et al., 2017; Verharen et al., 2019).
608 Previous studies have shown that PL neurons fire in response to shock-paired
609 cues and such activity is highly correlated with the expression of freezing responses
610 (Burgos-Robles et al., 2009; Sotres-Bayon et al., 2012; Kim et al., 2013; Courtin et al.,
611 2014). Adding to these findings, our recordings demonstrated that the activity of a small
612 number of PL neurons correlated with the onset of freezing responses, with the same
613 proportion of freezing-responsive cells being classified as PL^{GLUT} or PL^{GABA} neurons
614 (~10%). At first sight, the lack of effects on freezing behavior following optogenetic
615 activation of PL^{GLUT} neurons seems at odds with our recordings. It also seems to
616 disagree with previous studies showing that electrical stimulation or optogenetic
617 induction of 4Hz oscillations in PL increases conditioned freezing responses (Vidal-
618 Gonzalez et al., 2006; Courtin et al., 2014) by synchronizing the neural activity between

619 PL and BLA regions (Karalis et al., 2016). However, one important difference between
620 our study and others is that photoactivation of PL^{GLUT} neurons in our experiments was
621 performed in naïve rats, in the absence of shock-paired cues. Thus, the increased
622 freezing responses following PL activation reported in previous studies appear to be
623 dependent on the preexistence of a conditioned threat memory.

624 Overall, our results outline the neural correlates of risk-taking and risk-avoiding
625 behaviors in PL and reveal an important role for PL^{GLUT} neurons in coordinating
626 memory-based risky decision-making during conflict situations. Further studies will
627 focus on identifying the PL downstream/upstream circuits that regulate reward-
628 approaching and threat-avoidance responses, as well as the potential genetic and
629 epigenetic factors that could contribute to the observed behavioral phenotypes.
630 Elucidating the underlying mechanisms that mediate risk-taking vs. risk-avoiding
631 responses during situations of uncertainty may help to provide understanding of
632 response selection and adaptive behaviors, and may have clinical relevance to many
633 psychiatric disorders (Aupperle and Paulus, 2010; Kirlic et al., 2017). Whereas
634 persistent avoidance of presumed threats is the cardinal symptom of anxiety disorders
635 (Treanor and Barry, 2017), seeking reward despite negative consequences is a
636 hallmark of both eating and substance use disorders in humans (Volkow et al., 2012).
637

638 **ACKNOWLEDGEMENTS**

639 We thank Dr. Roger Janz for helping us with the packaging of the AAV-mDLX-ChR2-
640 mCherry viral construct, and Maria Nasheed, Ryia Albert and Sharon Gordon for their
641 technical assistance. We also thank current and former members of the Do Monte and

Quirk Labs for their valuable comments on the manuscript, and the Mind the Graph team for creating the schematic drawings presented in the manuscript. This work was supported by NIH grants R00-MH105549 and R01-MH120136, a Brain & Behavior Research Foundation grant (NARSAD Young Investigator), and a Rising STARs Award from UT System to F.H.D-M.

Author contributions

J.A.F-L., D.S.E., and G.A.M. performed the behaviors, optogenetics, and single-unit recordings. D.S.E. carried out the immunohistochemical and *in situ* hybridization studies. A.G. wrote and validated the DeepLabCut and the Python codes for behavioral analyses. J.A.F-L. wrote the MATLAB and Python codes for single-unit recording analyses. Both J.A.F-L. and F.H.D-M. analyzed the single-unit recording data. D.S.E. performed the statistical analyses. All the authors helped to design the study and interpret the data. J.A.F-L. and F.H.D-M. prepared the manuscript with comments from all the co-authors.

Competing interests

The authors declare no competing interests.

Correspondence and requests for materials should be addressed to F.H.D-M.

METHODS

Animals. All experimental procedures were approved by the Center for Laboratory Animal Medicine and Care of The University of Texas Health Science Center at Houston. The National Institutes of Health guidelines for the care and use of laboratory animals were strictly followed to minimize any potential discomfort and suffering of the animals. Male Long-Evans hooded adult rats (Charles Rivers Laboratories) with 3-5 months of age and weighing 300-450 g at the time of the experiment were used. Rats were single-housed and after a 3-day acclimation period handled and trained to press a lever for sucrose as described below. Animals were kept in a 12-hour light/12-hour dark cycle (light from 7:00 to 19:00) and maintained on a restricted diet of 18 g of standard laboratory rat chow provided daily at end of experimentation. Animals were given *ad libitum* access to water. Animals' weights were monitored weekly to ensure all animals maintained their weight under food restriction. During pre- and post- surgery phases, animals were given *ad libitum* access to food for a total of 7 days.

Surgeries. Rats were anaesthetized with 5% isoflurane in an induction chamber. Animals were positioned in a stereotaxic frame (Kopf Instruments) and anesthesia was maintained with 2.5% isoflurane delivered through a facemask. A heating pad was positioned bellow the body of the animal and both temperature and respiration were monitored during the entire surgery. Veterinary lubricant ointment was applied on the eyes to avoid dryness during the surgery. Animals received a subcutaneous injection of the local anesthetic bupivacaine (0.25%, 0.3 ml) at the incision site. Iodine and ethanol (70%) were alternately applied for asepsis of the incision site. The surgery procedures varied according to the type of implantation/injection (see below). For injection-only

688 surgeries, the incision was stitched after the injection by using surgical suture (Nylon, 3-
689 0). For implantation surgeries, the implants were fixed to the skull using C&B metabond
690 (Parkell), ortho acrylic cement, and four to six anchoring screws. After surgery, animals
691 received a subcutaneous injection of meloxicam (1 mg/Kg) and a topical triple antibiotic
692 was applied to the incision area.

693 **Viral vector injection.** Viral injections were performed using a microsyringe (SGE, 0.5
694 µl) with an injection rate of 0.04 µl/min plus an additional waiting time of 12 min to avoid
695 back-flow. The adeno-associated virus (AAV) was bilaterally injected at a volume of 0.4
696 µl per side. The AAV-CaMKIIα-eNpHR-eYFP vector was used to inhibit glutamatergic
697 neurons, whereas AAV-mDlx-ChR2–mCherry or AAV-CaMKIIα-ChR2-eYFP vectors
698 were used to activate either GABAergic or glutamatergic neurons, respectively. The use
699 of mDlx or CaMKIIα promoters enabled transgene expression favoring either
700 GABAergic or glutamatergic neurons, as previously shown (Gradinaru et al., 2009; Tye
701 et al., 2011; Dimidschstein et al., 2016; Sun et al., 2020) and was confirmed by our
702 immunohistochemical and RNAscope assessment **(Supplementary Fig. 4)**. The viral
703 construct AAV-CaMKIIα-eYFP was used to control for any nonspecific effects of viral
704 infection or laser heating. All plasmid or viral vectors were obtained from Addgene or
705 University of North Carolina Viral Vector Core. For implantation of optrodes, the
706 following coordinates from bregma were used for virus injection: PL, +2.7 mm AP, ±0.7
707 mm ML, -3.8 mm DV at a 0º angle. For PL soma illumination, an optical fiber (0.39 NA,
708 200 nm core, Inper) was implanted in each hemisphere targeting PL neurons using the
709 following coordinates from bregma: +2.7 mm AP; ±1.5 mm ML; -4.0 mm DV at a 15º
710 angle.

711

712 **Single-unit electrodes.** An array of 16 or 32 microwires was unilaterally implanted
713 targeting the PL using the following coordinates from bregma: +2.7 mm AP, ±0.8 mm
714 ML, -3.9 mm DV. Three different electrode configurations were used: i) 32-channel
715 silicon probes (Buzsaki32-CM32 or A1x32-5mm-25-177-CM32, Neuro Nexus
716 Technologies, USA), ii) Micro-Wire Arrays (MWA) of 16 or 32 channels (Bio-Signal
717 Technologies Ltd, USA); or iii) custom designed electrodes with 2×8 grid with 150 μm of
718 space between wires, 200 μ of space between rows, with 35 μm diameter wires
719 (Innovative Neurophysiology Inc., USA). For photoidentification of GABAergic or
720 glutamatergic neurons, a Hermes 32 channels optrode array was used (200 nm core,
721 Bio-Signal Technologies Ltd). Optrodes were unilaterally implanted at the same
722 coordinates described above after the infusion of 0.6 μl of AAV-mDlx-ChR2–mCherry or
723 AAV-CaMKIIα-ChR2-eYFP vectors. In all cases, the ground wire was wrapped around a
724 grounding screw previously anchored into the skull. Two insulated metal hooks were
725 implanted bilaterally into the cement to allow firmly attachment of the array connector to
726 the cable during recording.

727 **Odor preparation.** A 99% amyl acetate solution (Sigma Aldrich) was diluted in
728 propylene glycol (Bluewater Chemgroup, Inc) to a 10% solution and presented to the
729 rats during the different stages and phases of the olfactory threat conditioning test. A
730 customized olfactometer (Med Associates) was used to control the flow of air into the
731 animal's chamber. Before being mixed with the 10% amyl acetate solution, the air was
732 passed through a desiccant and a charcoal filter to remove any moisture and odors, and
733 was finally rehydrated with distilled water before being delivered into the chamber

through a thermoplastic PVC-based tube (Tygon) attached to an odor port located in the odor area.

Behavioral Tasks

Lever-press training. Rats were placed in a plexiglass, standard operant box (34 cm high x 25 cm wide x 23 cm deep, Med Associates), and trained to press a lever for sucrose on a fixed ratio of one pellet for each press. Next, animals were trained in a variable interval schedule of reinforcement that was gradually reduced across the days (one pellet every 15 s, 30 s, or 60 s) until the animals reached a minimum criterion of 10 presses/min. All sessions lasted 30 min and were performed on consecutive days. Sucrose pellet delivery, variable intervals, and session duration were controlled by an automated system (ANY-maze, Stoelting). Lever-press training lasted approximately one week, after which animals were assigned to surgery or cued food-seeking training. A small number of rats failed to reach the lever press criteria and were excluded from the experiments (< 3%).

Cued food-seeking training. Rats previously trained to press a lever for sucrose were trained to learn that each lever press in the presence of an audiovisual cue (tone: 3 KHz, 75 dB; light: yellow, 2.8 W; 30 s duration) resulted in the delivery of a sucrose pellet into a nearby dish. Reward cue conditioning also took place in the standard operant boxes. While the light cue helps to direct the animals toward the lever during the beginning of the training phase, the tone assures that the animals will not miss the presentation during the trial and provides the temporal precision required for single-unit recordings. After ~4 consecutive days of training (24 trials per day, pseudorandom intertrial interval of ~120 s, 60 min session), rats learned to discriminate the food-

associated cue as indicated by a significant increase in press rate during the presence of the audiovisual cues, when compared to the 30 s immediately before the cue onset (cue-off, see **Supplementary Fig. 1A**). The cued food-seeking training was completed when animals reached 50% of discriminability index (presses during cue-on period minus presses during cue-off period divided by the total number of presses). After the cued food-seeking training was completed, rats with single-unit electrodes were exposed to an additional training session in which the audiovisual cue ceased immediately after the animals pressed the lever and a single sucrose pellet was delivered into the dish. This extra training reduced the rat's response to a single press and dish entry per cue, thereby enabling us to correlate each food-seeking event with the neuronal firing rate by avoiding overlapping between consecutive events (e.g., lever presses). The single-pellet training took place in the same plexiglass rectangular arena subsequently used for the odor test (40 cm high x 60 cm wide x 26 cm deep, Med Associates, see schematic in **Fig. 1A right**). The arena consisted of a hidden area (40 cm high x 20 cm wide x 26 cm deep) separated from an open area by a plexiglass division. An 8-cm slot located in the center of the division enabled the animal to transition between both sides of the arena. For behavioral quantification, the open area was subdivided into a center area and a food area (40 cm high x 12 cm wide x 26 cm deep), the latter containing a lever, a dish, and an external feeder similar to the food-seeking operant box.

Habituation day. Animals were placed in the odor arena and exposed to 12 audiovisual cues (30 s duration, pseudorandom inter-trial intervals of between 25-40 s) followed by 10 min of presentation to the neutral odor alone (10% amyl acetate) and an additional

12 audiovisual cues similar to the first cues but in the presence of the neutral odor delivered in the food area of the arena. Each lever press in the presence of the audiovisual cue resulted in the delivery of a sucrose pellet into the dish, and the audiovisual cue was ceased immediately after the animal pressed the lever.

Threat *conditioning day.* One day after the habituation day, rats were placed in a plexiglass, standard operant box similar to the cued food-seeking training box, but with the grid floor previously attached to a shock generator system. Rats were habituated to one nonreinforced odor presentation (10% amyl acetate, 30 s duration) followed by five odor presentations that coterminated with a foot shock (0.7 mA, 1 s duration, 258-318 s inter-trial intervals). An olfactometer system was used to precisely deliver the odor into the box (see odor preparation session above), whereas an exhaustor system was used to remove the odor from the box during the intertrial intervals. Between each odor presentation, audiovisual cues (30 s duration) signaling the availability of sucrose were presented to the animals. Each lever press during the audiovisual cues resulted in the delivery of a sucrose pellet into the dish. Shock grids and floor trays were cleaned with 70% ethanol between each rat.

Test day. One day after the threat conditioning session, rats were returned to the same arena used during the habituation and exposed to the exact same protocol. The first phase of the test session was called *reward phase* and the animals were exposed to 12 food cues. The second phase was called *odor phase* and the animals were exposed to 10 min of conditioned odor (10% amyl acetate) alone. The last phase was called *conflict phase* and the animals were exposed to 12 food cues in the presence of the conditioned odor. In order to press the lever for sucrose during the conflict phase, rats had to

803 approach the conditioned odor presented in the food area. After the end of the conflict
804 phase, the odor was extracted from the arena with an exhaustor and the floor and walls
805 of the arena were cleaned thoroughly with 70% ethanol solution.

806 **Behavioral tracking.** Both the standard operant boxes and the testing arenas were
807 equipped with video cameras and a behavior tracking software (ANY-maze, Stoelting)
808 which were used to record the animal's behavior and control the delivery of sucrose,
809 foot shock, tone, light and odor in the apparatuses. Avoidance responses were
810 characterized by the time spent in the hidden area of the arena. Freezing responses
811 were characterized by the complete absence of movements except those needed for
812 respiration. Risk-assessment responses were characterized by a body stretching
813 movement to peep out toward the food area while in the hidden area and were used as
814 a measure of risk-assessment behavior (Blanchard et al., 2011).

815 For single-unit recording analyses, the detection of freezing, avoidance and risk
816 assessment behaviors were performed using the open source tool DeepLabCut, a
817 machine learning software that tracks complex patterns of behavior from videos (Mathis
818 et al., 2018). After a video has been analyzed, the data was saved to a .csv file that
819 contained the x and y location of each rat's body part in pixels, as well as the analysis of
820 the expected accuracy (i.e., likelihood) of the tracked positions across time. After
821 DeepLabCut has calculated the positions and the likelihood, we used three different
822 Python codes to identify each one of the three behaviors. For freezing behavior, the
823 code used DeepLabCut's position data and determined if the rat was still for more than
824 500 ms. The animal was considered to be still if the position in question was within 1.05
825 pixels of each other. For avoidance behavior, the code used DeepLabCut's position

826 data to determine the location of the rat in the arena and based on the center of its head
827 to identify when the animals entered the hidden area of the arena. Finally, for risk
828 assessment behavior, the code used DeepLabCut's position data to identify the nose,
829 ears, center of the head, and spine to determine whether the rat was located in the
830 hidden area of the arena with its body stretched and the head looking through the open
831 division of the apparatus. Each of these codes generated a .xlsx file that contained the
832 onset and the total duration of each behavioral episode. The time onsets for each
833 behavior were filtered by selecting only the events that lasted more than 1 second and
834 were not preceded by the same behavior during the previous 6 s (baseline). The final
835 list of time onsets was entered into the single-unit recording files to create the events
836 and temporally align them with the neuronal recordings.

837 **Optogenetic stimulation during behavior.** Bilateral optical cables (200 μm core, 0.37
838 NA, 2.5 mm ceramic ferrule, Inper) were connected to a blue laser (diode-pumped solid-
839 state, 473 nm, 150 mW output, OptoEngine) or a yellow laser (diode-pumped solid-
840 state, 593.5 nm, 300 mW output, OptoEngine) by using a patch cord (200 μm, 0.39 NA,
841 FC/PC connector, Inper) through a dual rotary joint (200 μm core, Doric lenses). During
842 the stimulation, the optical cables were coupled to the previously implanted optical
843 fibers by using a ceramic sleeve (2.5 mm, Precision Fiber Products). An optogenetic
844 interface (Ami-2, Stoelting) and an electrical stimulator (Master 9, A.M.P. Instruments)
845 were used to control the onset of the laser, pulse width, train duration, and frequency.
846 The power density estimated at the tip of the optical fiber was 7-10 mW for illumination
847 of PL somata (PM-100D, Power Energy Meter, Thor Labs).

848 **Single-unit recording.** A 64-channels neuronal data acquisition system (Omniplex,
849 Plexon) integrated with a high-resolution video-tracking system (Cineplex, Plexon) was
850 used for electrophysiological recordings from freely behaving animals. Both videos and
851 neuronal recordings were combined within the same file, thereby facilitating the
852 correlation of behavior with neuronal activity. An electrical isolation, Faraday cage was
853 made and connected to the grounding port of the data acquisition system. The system
854 was connected to the head-mounted electrode/optrode by using a digital headstage
855 cable (32 channels, Plexon), a motorized carrousel commutator (Plexon), and a digital
856 headstage processor (Plexon). Rats were habituated to the headstage cable daily for
857 approximately one week before the beginning of the experiments. Extracellular
858 waveforms exceeding a voltage threshold were band-pass filtered (500 - 5,000 Hz),
859 digitized at 40 KHz, and stored onto disk. Automated processing was performed using a
860 valley-seeking scan algorithm and then visually evaluated using sort quality metrics
861 (Offline Sorter, Plexon). Single-units were selected based on three principal
862 components and waveform features such as valley-to-peak and amplitude
863 measurements. A commercial software (NeuroExplorer, NEXT Technologies), Matlab
864 (MathWorks) scripts, and Python scripting in NeuroExplorer were implemented to
865 calculate the spontaneous firing rate and food-cue responses. The spontaneous firing
866 rate was calculated by comparing the frequency of spike trains during the last 30 s of
867 the food-seeking phase, odor phase, or conflict phase against the 30 s prior to the
868 beginning of each session. Food cue responses were calculated by implementing
869 Matlab scripts as Z-scores normalized to 20 pre-cue bins of 300 ms. Neurons showing a
870 Z-score > 2.58 ($p < 0.01$) during the first two-bins following the onset of the food cues

871 were classified as excitatory responses, whereas neurons showing a Z-score < -1.96 (p
872 < 0.05) during the same first two-bins were classified as inhibitory responses. At the end
873 of the recording sessions, a micro-lesion was made by passing anodal current (0.3 mA
874 for 15 s) through the active wires to deposit iron in the tissue. After perfusion, brains
875 were extracted from the skull and stored in a 30% sucrose/ 6% ferrocyanide solution to
876 stain the iron deposits.

877 **Photoidentification of PL neurons during recordings.** During neuronal
878 photoidentification, we recorded from rats expressing channelrhodopsin (ChR2) in PL
879 neurons previously implanted with an optrode in the same region. An optical cable
880 connected to a blue laser was attached to the headstage cable and coupled to the
881 previously implanted optical fiber by using a ceramic sleeve. At the end of the
882 behavioral session, 10 trains of 10-s blue laser pulses (5 ms pulse width, 5 Hz) were
883 delivered by a Master-9 programmable pulse stimulator, which also sent flags to the
884 data acquisition system to mark the time of the laser events. Neurons were considered
885 to be responsive to photostimulation if they showed a significant increase in firing rate
886 above baseline (20 ms, Z-score > 3.29, p < 0.001) within the 6 ms (for PL^{GLUT} neurons)
887 or 12 ms (for PL^{GABA} neurons) after laser, similar to previous studies (Lima et al., 2009;
888 Pi et al., 2013; Burgos-Robles et al., 2017; Engelke et al., 2021).

889 **Optogenetic manipulation of PL neurons during behavior.** During the cued food-
890 seeking test, rats expressing ChR2 or eNpHR in PL were bilaterally illuminated in the
891 same region by using a blue (5 ms pulse width, 5 Hz for CaMKIIα or 20 Hz for mDlx) or
892 a yellow laser (constant illumination), respectively. The laser was activated at cue onset
893 and persisted throughout the entire 30 s of the audiovisual cue presentation. Rats were

894 exposed to two consecutive cues with laser off followed by two consecutive cues with
895 laser on in a total of 12 cues (pseudorandom inter-trial intervals of between 25-40 s). To
896 assess the effects of PL illumination on rat's defensive behavior, PL neurons of rats
897 expressing ChR2 or eNpHR were bilaterally illuminated during 6 distinct epochs of 30 s
898 during the *odor phase* by using a blue (5 ms pulse width, 20 Hz) or a yellow laser
899 (constant illumination), respectively. To assess the effects of PL illumination on food-
900 seeking responses during the *conflict phase*, rats were exposed to two consecutive
901 cues with laser off followed by two consecutive cues with laser on in a total of 12 cues
902 (pseudorandom inter-trial intervals of between 25-40 s). The laser was activated at cue
903 onset and persisted on until the animal pressed the bar or the 30 s of the audiovisual
904 cue was completed.

905 **Histology.** Animals were transcardially perfused with KPBS followed by 10% buffered
906 formalin. Brains were processed for histology as previously described (Do-Monte et al.,
907 2013). Only rats with the presence of eYFP or mCherry labeling and the track of the
908 electrode wires or optical fiber tips located exclusively in PL were included in the
909 statistical analyses.

910 **Immunohistochemistry.** Rats previously infused with AAV-mDlx-ChR2-mCherry or
911 AAV-CaMKIIα-ChR2-eYFP were transcardially perfused with KPBS followed by 10%
912 buffered formalin. Brains were removed from the skull, transferred to a 20% sucrose
913 solution in KPBS for 24 h, and stored in a 30% sucrose solution in KPBS for another 24
914 h. Next, coronal PL sections (40 μm thick) were cut in a cryostat (CM 1860, Leica),
915 blocked in 20% normal goat serum and 0.3% Triton X-100 in KPBS at room
916 temperature for 1 h. For identification of GABAergic neurons, PL sections were

917 incubated with anti-GAD67 serum raised in rabbit (1:400; Millipore-Sigma) at 4°C for 48
918 h. After sections were washed in KPBS for 5 times, sections were incubated with a
919 secondary anti-rabbit antibody (1:200, Alexa Fluor 488 or Alexa Fluor 594, Abcam) for 2
920 h. Sections were washed with KPBS, mounted in Superfrost Plus slides, and
921 coverslipped with anti-fading mounting medium (Vectashield, Vectorlabs). Images were
922 generated by using a microscope (Nikon, Eclipse NiE Fully Motorized Upright
923 Microscope) equipped with a fluorescent lamp (X-Cite, 120 LED) and a digital camera
924 (Andor Zyla 4.2 PLUS sCMOS).

925 ***In situ* hybridization.** Single molecule fluorescent *in situ* hybridization (RNAscope
926 Multiplex Fluorescent Detection Kit v2, Advanced Cell Diagnostics) was used following
927 the manufacturer protocol for fixed-frozen brains sample. Brain samples were sectioned
928 at a thickness of 20 μm in a cryostat (CM1860, Leica). Sections were collected onto
929 superfrost plus slides (Fisher Scientific) and transferred to a −80°C freezer. To prepare
930 for the assay, brain sections were serially dehydrated with EtOH (50%, 75%, and 100%,
931 each for 5 min) and then incubated in hydrogen peroxide for 10 min. Target retrieval
932 was performed with RNAscope target retrieval reagents at 99°C for 5 min. The sections
933 were then pretreated with Protease III (RNAScope) for 40 min at 40°C. RNAscope
934 probes (Advanced Cell Diagnostics) for mCherry (Cat No. 431201-C3) and vGAT (Cat
935 No. 424541) were hybridized at 40°C for 2h, serially amplified, and revealed with
936 horseradish peroxidase, Opal Dye/TSA Plus fluorophore (Akoya Biosciences), and
937 horseradish peroxidase blocker. Sections were cover-slipped with anti-fading mounting
938 medium with DAPI (Vectashield, Vectorlabs) and kept in the refrigerator. Images were
939 generated by using an epifluorescent microscope (Nikon, Eclipse NiE Fully Motorized

Upright Microscope) equipped with a fluorescent lamp (X-Cite, 120 LED) and a digital camera (Andor Zyla 4.2 PLUS sCMOS). Expression of mCherry mRNA (red, Opal 620) and GAD67 mRNA (green, Opal 520) was determined by using an automated fluorescent threshold detector (NIS-Elements). Colabeled cells were manually counted by an experimenter by measuring either the percentage of mCherry positive neurons in PL that were also labeled with GAD67, or the percentage of GAD67 positive neurons in PL that were also labeled with mCherry.

Data analyses

Behavioral quantification and statistical analysis. Rats were recorded with digital video cameras (Logitech C920) and behavioral responses were measured by using an automated video-tracking system (ANY-maze) or machine learning (DeepLabCut). Presses per minute were calculated by measuring the number of presses during the 30 s cue multiplied by two. All graphics and numerical values reported in the figures are presented as mean ± s.e.m. Statistical significance was determined with paired or unpaired Student's t test, repeated-measures ANOVA followed by Bonferroni post-hoc comparisons (Prism 7), and Z-test or Fisher's exact test, as indicated in Table 1S. Sample size was based on estimations by power analysis with a level of significance of 0.05 and a power of 0.9.

Single-unit analyses. Based on data from NeuroExplorer, waveform data and spike timestamps for firing rates was processed through Matlab scripting. The principal-component scores for unsorted waveforms were computed and plotted in a three (or two) dimensional principal-component space. Clusters containing similar valid waveforms were manually defined. After manually clustering similar valid waveforms, a

963 group of spikes were considered from a single neuron if the waveforms formed a
964 discrete, isolated, cluster in the principal-component space. The separation of putative
965 PL^{GLUT} neurons and putative PL^{GABA} neurons was made through an unbiased
966 unsupervised cluster-separation algorithm based on two electrophysiological properties:
967 neuron's average half-spike width (ms) and firing rate (Hz) (Frank et al., 2001). Only *in*
968 *vivo* photoidentified PL neurons (i.e., GABAergic or glutamatergic) were considered for
969 these analyses. To separate putative PL^{GLUT} neurons and putative PL^{GABA} we used an
970 unsupervised cluster algorithm based on Matlab's k-means++ algorithm for centroid
971 initialization and squared Euclidean distance (Arthur and Vassilvitskii, 2007). The
972 Euclidian distance was calculated between all neuron pairs to detect 2 clusters on the
973 two-dimensional space defined by each cluster representing putative GABAergic or
974 glutamatergic neurons.

975 Data availability

976 All the data that support the findings presented in this study are available from the
977 corresponding author on reasonable request.

978
979
980
981
982
983
984
985
986
987

988 **REFERENCES**

989

990 Ainslie G (1975) Specious reward: a behavioral theory of impulsiveness and impulse
991 control. Psychol Bull 82:463-496.
992 Amir A, Lee SC, Headley DB, Herzallah MM, Pare D (2015) Amygdala Signaling during
993 Foraging in a Hazardous Environment. J Neurosci 35:12994-13005.
994 Arthur D, Vassilvitskii S (2007) K-means++: The Advantages of Careful Seeding. SODA
995 '07: Proceedings of the Eighteenth Annual ACM-SIAM Symposium on Discrete
996 Algorithms:1027-1035.
997 Aupperle RL, Paulus MP (2010) Neural systems underlying approach and avoidance in
998 anxiety disorders. Dialogues Clin Neurosci 12:517-531.
999 Baeg EH, Kim YB, Jang J, Kim HT, Mook-Jung I, Jung MW (2001) Fast spiking and
1000 regular spiking neural correlates of fear conditioning in the medial prefrontal
1001 cortex of the rat. Cereb Cortex 11:441-451.
1002 Bari A, Theobald DE, Caprioli D, Mar AC, Aidoo-Micah A, Dalley JW, Robbins TW
1003 (2010) Serotonin modulates sensitivity to reward and negative feedback in a
1004 probabilistic reversal learning task in rats. Neuropsychopharmacology 35:1290-
1005 1301.
1006 Barker TV, Buzzell GA, Fox NA (2019) Approach, avoidance, and the detection of
1007 conflict in the development of behavioral inhibition. New Ideas Psychol 53:2-12.
1008 Bartho P, Hirase H, Monconduit L, Zugaro M, Harris KD, Buzsaki G (2004)
1009 Characterization of neocortical principal cells and interneurons by network
1010 interactions and extracellular features. J Neurophysiol 92:600-608.
1011 Becchetti A, Gullo F, Bruno G, Dossi E, Lecchi M, Wanke E (2012) Exact distinction of
1012 excitatory and inhibitory neurons in neural networks: a study with GFP-GAD67
1013 neurons optically and electrophysiologically recognized on multielectrode arrays.
1014 Front Neural Circuits 6:63.
1015 Berglind WJ, See RE, Fuchs RA, Ghee SM, Whitfield TW, Jr., Miller SW, McGinty JF
1016 (2007) A BDNF infusion into the medial prefrontal cortex suppresses cocaine
1017 seeking in rats. Eur J Neurosci 26:757-766.
1018 Beyeler A, Namburi P, Glober GF, Simonnet C, Calhoon GG, Conyers GF, Luck R,
1019 Wildes CP, Tye KM (2016) Divergent Routing of Positive and Negative
1020 Information from the Amygdala during Memory Retrieval. Neuron 90:348-361.
1021 Blanchard DC, Griebel G, Pobbe R, Blanchard RJ (2011) Risk assessment as an
1022 evolved threat detection and analysis process. Neurosci Biobehav Rev 35:991-
1023 998.
1024 Bravo-Rivera H, Rubio Arzola P, Caban-Murillo A, Velez-Aviles AN, Ayala-Rosario SN,
1025 Quirk GJ (2021) Characterizing Different Strategies for Resolving Approach-
1026 Avoidance Conflict. Front Neurosci 15:608922.
1027 Breton JM, Charbit AR, Snyder BJ, Fong PTK, Dias EV, Himmels P, Lock H, Margolis
1028 EB (2019) Relative contributions and mapping of ventral tegmental area
1029 dopamine and GABA neurons by projection target in the rat. J Comp Neurol
1030 527:916-941.

1031 Burgos-Robles A, Vidal-Gonzalez I, Quirk GJ (2009) Sustained conditioned responses
1032 in prelimbic prefrontal neurons are correlated with fear expression and extinction
1033 failure. J Neurosci 29:8474-8482.
1034 Burgos-Robles A, Bravo-Rivera H, Quirk GJ (2013) Prelimbic and infralimbic neurons
1035 signal distinct aspects of appetitive instrumental behavior. PLoS One 8:e57575.
1036 Burgos-Robles A, Kimchi EY, Izadmehr EM, Porzenheim MJ, Ramos-Guasp WA, Nieh
1037 EH, Felix-Ortiz AC, Namburi P, Leppla CA, Presbrey KN, Anandalingam KK,
1038 Pagan-Rivera PA, Anahtar M, Beyeler A, Tye KM (2017) Amygdala inputs to
1039 prefrontal cortex guide behavior amid conflicting cues of reward and punishment.
1040 Nat Neurosci.
1041 Cain CK (2019) Avoidance Problems Reconsidered. Curr Opin Behav Sci 26:9-17.
1042 Capuzzo G, Floresco SB (2020) Prelimbic and Infralimbic Prefrontal Regulation of
1043 Active and Inhibitory Avoidance and Reward-Seeking. J Neurosci 40:4773-4787.
1044 Chen BT, Yau HJ, Hatch C, Kusumoto-Yoshida I, Cho SL, Hopf FW, Bonci A (2013)
1045 Rescuing cocaine-induced prefrontal cortex hypoactivity prevents compulsive
1046 cocaine seeking. Nature 496:359-362.
1047 Choi EA, McNally GP (2017) Paraventricular Thalamus Balances Danger and Reward.
1048 J Neurosci 37:3018-3029.
1049 Choi EA, Jean-Richard-Dit-Bressel P, Clifford CWG, McNally GP (2019) Paraventricular
1050 Thalamus Controls Behavior during Motivational Conflict. J Neurosci 39:4945-
1051 4958.
1052 Cohen JY, Haesler S, Vong L, Lowell BB, Uchida N (2012) Neuron-type-specific signals
1053 for reward and punishment in the ventral tegmental area. Nature 482:85-88.
1054 Constantinidis C, Goldman-Rakic PS (2002) Correlated discharges among putative
1055 pyramidal neurons and interneurons in the primate prefrontal cortex. J
1056 Neurophysiol 88:3487-3497.
1057 Courtin J, Chaudun F, Rozeske RR, Karalis N, Gonzalez-Campo C, Wurtz H, Abdi A,
1058 Baufreton J, Bienvenu TC, Herry C (2014) Prefrontal parvalbumin interneurons
1059 shape neuronal activity to drive fear expression. Nature 505:92-96.
1060 Cummings KA, Clem RL (2020) Prefrontal somatostatin interneurons encode fear
1061 memory. Nat Neurosci 23:61-74.
1062 Dejean C, Courtin J, Karalis N, Chaudun F, Wurtz H, Bienvenu TC, Herry C (2016)
1063 Prefrontal neuronal assemblies temporally control fear behaviour. Nature
1064 535:420-424.
1065 Dellu-Hagedorn F, Rivalan M, Fitoussi A, De Deurwaerdere P (2018) Inter-individual
1066 differences in the impulsive/compulsive dimension: deciphering related
1067 dopaminergic and serotonergic metabolisms at rest. Philos Trans R Soc Lond B
1068 Biol Sci 373.
1069 Diehl MM, Bravo-Rivera C, Rodriguez-Romaguera J, Pagan-Rivera PA, Burgos-Robles
1070 A, Roman-Ortiz C, Quirk GJ (2018) Active avoidance requires inhibitory signaling
1071 in the rodent prelimbic prefrontal cortex. Elife 7.
1072 Dimidschstein J et al. (2016) A viral strategy for targeting and manipulating interneurons
1073 across vertebrate species. Nat Neurosci 19:1743-1749.
1074 Do-Monte FH, Quinones-Laracuente K, Quirk GJ (2015) A temporal shift in the circuits
1075 mediating retrieval of fear memory. Nature 519:460-463.

1076 Do-Monte FH, Rodriguez-Romaguera J, Rosas-Vidal LE, Quirk GJ (2013) Deep brain
1077 stimulation of the ventral striatum increases BDNF in the fear extinction circuit.
1078 Front Behav Neurosci 7:102.
1079 Do Monte FH, Quirk GJ, Li B, Penzo MA (2016) Retrieving fear memories, as time goes
1080 by. Mol Psychiatry 21:1027-1036.
1081 Emmons EB, Ruggiero RN, Kelley RM, Parker KL, Narayanan NS (2016) Corticostriatal
1082 Field Potentials Are Modulated at Delta and Theta Frequencies during Interval-
1083 Timing Task in Rodents. Front Psychol 7:459.
1084 Engelke DS, Zhang XO, O'Malley JJ, Fernandez-Leon JA, Li S, Kirouac GJ, Beierlein
1085 M, Do-Monte FH (2021) A hypothalamic-thalamostriatal circuit that controls
1086 approach-avoidance conflict in rats. Nat Commun 12:2517.
1087 Fan H, Pan X, Wang R, Sakagami M (2017) Differences in reward processing between
1088 putative cell types in primate prefrontal cortex. PLoS One 12:e0189771.
1089 Ferenczi EA, Zalocusky KA, Liston C, Grosenick L, Warden MR, Amatya D, Katovich K,
1090 Mehta H, Patenaude B, Ramakrishnan C, Kalanithi P, Etkin A, Knutson B, Glover
1091 GH, Deisseroth K (2016) Prefrontal cortical regulation of brainwide circuit
1092 dynamics and reward-related behavior. Science 351:aac9698.
1093 Flagel SB, Watson SJ, Robinson TE, Akil H (2007) Individual differences in the
1094 propensity to approach signals vs goals promote different adaptations in the
1095 dopamine system of rats. Psychopharmacology (Berl) 191:599-607.
1096 Flagel SB, Clark JJ, Robinson TE, Mayo L, Czuj A, Willuhn I, Akers CA, Clinton SM,
1097 Phillips PE, Akil H (2011) A selective role for dopamine in stimulus-reward
1098 learning. Nature 469:53-57.
1099 Frank LM, Brown EN, Wilson MA (2001) A comparison of the firing properties of
1100 putative excitatory and inhibitory neurons from CA1 and the entorhinal cortex. J
1101 Neurophysiol 86:2029-2040.
1102 Gabbott PL, Warner TA, Jays PR, Salway P, Busby SJ (2005) Prefrontal cortex in the
1103 rat: projections to subcortical autonomic, motor, and limbic centers. J Comp
1104 Neurol 492:145-177.
1105 Gaykema RP, Nguyen XM, Boehret JM, Lambeth PS, Joy-Gaba J, Warthen DM, Scott
1106 MM (2014) Characterization of excitatory and inhibitory neuron activation in the
1107 mouse medial prefrontal cortex following palatable food ingestion and food driven
1108 exploratory behavior. Front Neuroanat 8:60.
1109 Geller I (1960) The acquisition and extinction of conditioned suppression as a function
1110 of the base-line reinforcer. J Exp Anal Behav 3:235-240.
1111 Gradinaru V, Mogri M, Thompson KR, Henderson JM, Deisseroth K (2009) Optical
1112 deconstruction of parkinsonian neural circuitry. Science 324:354-359.
1113 Haight JL, Fuller ZL, Fraser KM, Flagel SB (2017) A food-predictive cue attributed with
1114 incentive salience engages subcortical afferents and efferents of the
1115 paraventricular nucleus of the thalamus. Neuroscience 340:135-152.
1116 Harris AZ, Gordon JA (2015) Long-range neural synchrony in behavior. Annu Rev
1117 Neurosci 38:171-194.
1118 Hassani OK, Lee MG, Henny P, Jones BE (2009) Discharge profiles of identified
1119 GABAergic in comparison to cholinergic and putative glutamatergic basal
1120 forebrain neurons across the sleep-wake cycle. J Neurosci 29:11828-11840.

1121 Horst NK, Laubach M (2013) Reward-related activity in the medial prefrontal cortex is
1122 driven by consumption. Front Neurosci 7:56.
1123 Hu H (2016) Reward and Aversion. Annu Rev Neurosci 39:297-324.
1124 Hyman JM, Hasselmo ME, Seamans JK (2011) What is the Functional Relevance of
1125 Prefrontal Cortex Entrainment to Hippocampal Theta Rhythms? Front Neurosci
1126 5:24.
1127 Jean-Richard-Dit-Bressel P, Ma C, Bradfield LA, Killcross S, McNally GP (2019)
1128 Punishment insensitivity emerges from impaired contingency detection, not
1129 aversion insensitivity or reward dominance. Elife 8.
1130 Jensen J, Walter H (2014) Incentive motivational salience and the human brain. Restor
1131 Neurol Neurosci 32:141-147.
1132 Karalis N, Dejean C, Chaudun F, Khoder S, Rozeske RR, Wurtz H, Bagur S,
1133 Benchenane K, Sirota A, Courtin J, Herry C (2016) 4-Hz oscillations synchronize
1134 prefrontal-amygdala circuits during fear behavior. Nat Neurosci.
1135 Kim CK, Ye L, Jennings JH, Pichamoorthy N, Tang DD, Yoo AW, Ramakrishnan C,
1136 Deisseroth K (2017) Molecular and Circuit-Dynamical Identification of Top-Down
1137 Neural Mechanisms for Restraint of Reward Seeking. Cell 170:1013-1027 e1014.
1138 Kim EJ, Kim N, Kim HT, Choi JS (2013) The prelimbic cortex is critical for context-
1139 dependent fear expression. Front Behav Neurosci 7:73.
1140 Kim EJ, Kong MS, Park SG, Mizumori SJY, Cho J, Kim JJ (2018) Dynamic coding of
1141 predatory information between the prelimbic cortex and lateral amygdala in
1142 foraging rats. Sci Adv 4:eaar7328.
1143 Kirlic N, Young J, Aupperle RL (2017) Animal to human translational paradigms relevant
1144 for approach avoidance conflict decision making. Behav Res Ther 96:14-29.
1145 Kroener S, Chandler LJ, Phillips PE, Seamans JK (2009) Dopamine modulates
1146 persistent synaptic activity and enhances the signal-to-noise ratio in the
1147 prefrontal cortex. PLoS One 4:e6507.
1148 Krypotos AM, Effting M, Kindt M, Beckers T (2015) Avoidance learning: a review of
1149 theoretical models and recent developments. Front Behav Neurosci 9:189.
1150 Kyriazi P, Headley DB, Pare D (2020) Different Multidimensional Representations
1151 across the Amygdalo-Prefrontal Network during an Approach-Avoidance Task.
1152 Neuron 107:717-730 e715.
1153 Likhtik E, Paz R (2015) Amygdala-prefrontal interactions in (mal)adaptive learning.
1154 Trends Neurosci 38:158-166.
1155 Likhtik E, Stujenske JM, Topiwala MA, Harris AZ, Gordon JA (2014) Prefrontal
1156 entrainment of amygdala activity signals safety in learned fear and innate
1157 anxiety. Nat Neurosci 17:106-113.
1158 Lima SQ, Hromadka T, Znamenskiy P, Zador AM (2009) PINP: a new method of
1159 tagging neuronal populations for identification during in vivo electrophysiological
1160 recording. PLoS One 4:e6099.
1161 Marquis JP, Killcross S, Haddon JE (2007) Inactivation of the prelimbic, but not
1162 infralimbic, prefrontal cortex impairs the contextual control of response conflict in
1163 rats. Eur J Neurosci 25:559-566.
1164 Mathis A, Mamidanna P, Cury KM, Abe T, Murthy VN, Mathis MW, Bethge M (2018)
1165 DeepLabCut: markerless pose estimation of user-defined body parts with deep
1166 learning. Nat Neurosci 21:1281-1289.

1167 McDonald AJ (1991) Organization of amygdaloid projections to the prefrontal cortex and
1168 associated striatum in the rat. Neuroscience 44:1-14.
1169 McGinley MJ, David SV, McCormick DA (2015) Cortical Membrane Potential Signature
1170 of Optimal States for Sensory Signal Detection. Neuron 87:179-192.
1171 McGinty JF, Otis JM (2020) Heterogeneity in the Paraventricular Thalamus: The Traffic
1172 Light of Motivated Behaviors. Front Behav Neurosci 14:590528.
1173 McNaughton N, Corr PJ (2014) Approach, avoidance, and their conflict: the problem of
1174 anchoring. Front Syst Neurosci 8:124.
1175 Millan EZ, Ong Z, McNally GP (2017) Paraventricular thalamus: Gateway to feeding,
1176 appetitive motivation, and drug addiction. Prog Brain Res 235:113-137.
1177 Moorman DE, Aston-Jones G (2015) Prefrontal neurons encode context-based
1178 response execution and inhibition in reward seeking and extinction. Proc Natl
1179 Acad Sci U S A 112:9472-9477.
1180 Morales I, Berridge KC (2020) 'Liking' and 'wanting' in eating and food reward: Brain
1181 mechanisms and clinical implications. Physiol Behav 227:113152.
1182 Mruczek RE, Sheinberg DL (2012) Stimulus selectivity and response latency in putative
1183 inhibitory and excitatory neurons of the primate inferior temporal cortex. J
1184 Neurophysiol 108:2725-2736.
1185 Nair-Roberts RG, Chatelain-Badie SD, Benson E, White-Cooper H, Bolam JP, Ungless
1186 MA (2008) Stereological estimates of dopaminergic, GABAergic and
1187 glutamatergic neurons in the ventral tegmental area, substantia nigra and
1188 retrorubral field in the rat. Neuroscience 152:1024-1031.
1189 Namburi P, Beyeler A, Yorozu S, Calhoon GG, Halbert SA, Wichmann R, Holden SS,
1190 Mertens KL, Anahtar M, Felix-Ortiz AC, Wickersham IR, Gray JM, Tye KM (2015)
1191 A circuit mechanism for differentiating positive and negative associations. Nature
1192 520:675-678.
1193 Narayanan NS, Cavanagh JF, Frank MJ, Laubach M (2013) Common medial frontal
1194 mechanisms of adaptive control in humans and rodents. Nat Neurosci 16:1888-
1195 1895.
1196 Oberrauch S, Sigrist H, Sautter E, Gerster S, Bach DR, Pryce CR (2019) Establishing
1197 operant conflict tests for the translational study of anxiety in mice.
1198 Psychopharmacology (Berl) 236:2527-2541.
1199 Ono M, Bishop DC, Oliver DL (2017) Identified GABAergic and Glutamatergic Neurons
1200 in the Mouse Inferior Colliculus Share Similar Response Properties. J Neurosci
1201 37:8952-8964.
1202 Orsini CA, Heshmati SC, Garman TS, Wall SC, Bizon JL, Setlow B (2018) Contributions
1203 of medial prefrontal cortex to decision making involving risk of punishment.
1204 Neuropharmacology 139:205-216.
1205 Otis JM, Namboodiri VM, Matan AM, Voets ES, Mohorn EP, Kosyk O, McHenry JA,
1206 Robinson JE, Resendez SL, Rossi MA, Stuber GD (2017) Prefrontal cortex
1207 output circuits guide reward seeking through divergent cue encoding. Nature
1208 543:103-107.
1209 Padilla-Coreano N, Canetta S, Mikofsky RM, Alway E, Passecker J, Myroshnychenko
1210 MV, Garcia-Garcia AL, Warren R, Teboul E, Blackman DR, Morton MP, Hupalo
1211 S, Tye KM, Kellendonk C, Kupferschmidt DA, Gordon JA (2019) Hippocampal-

Prefrontal Theta Transmission Regulates Avoidance Behavior. Neuron 104:601-610 e604.
Park J, Moghaddam B (2017) Risk of punishment influences discrete and coordinated encoding of reward-guided actions by prefrontal cortex and VTA neurons. Elife 6.
Penzo MA, Gao C (2021) The paraventricular nucleus of the thalamus: an integrative node underlying homeostatic behavior. Trends Neurosci.
Pi HJ, Hangya B, Kvitsiani D, Sanders JI, Huang ZJ, Kepecs A (2013) Cortical interneurons that specialize in disinhibitory control. Nature 503:521-524.
Piantadosi PT, Yeates DCM, Floresco SB (2020) Prefrontal cortical and nucleus accumbens contributions to discriminative conditioned suppression of reward-seeking. Learn Mem 27:429-440.
Popa D, Duvarci S, Popescu AT, Lena C, Pare D (2010) Coherent amygdalocortical theta promotes fear memory consolidation during paradoxical sleep. Proc Natl Acad Sci U S A 107:6516-6519.
Radke AK, Nakazawa K, Holmes A (2015) Cortical GluN2B deletion attenuates punished suppression of food reward-seeking. Psychopharmacology (Berl) 232:3753-3761.
Robinson TE, Flagel SB (2009) Dissociating the predictive and incentive motivational properties of reward-related cues through the study of individual differences. Biol Psychiatry 65:869-873.
Robinson TE, Yager LM, Cogan ES, Saunders BT (2014) On the motivational properties of reward cues: Individual differences. Neuropharmacology 76 Pt B:450-459.
Sangha S, Robinson PD, Greba Q, Davies DA, Howland JG (2014) Alterations in reward, fear and safety cue discrimination after inactivation of the rat prelimbic and infralimbic cortices. Neuropsychopharmacology 39:2405-2413.
Santana N, Bortolozzi A, Serrats J, Mengod G, Artigas F (2004) Expression of serotonin1A and serotonin2A receptors in pyramidal and GABAergic neurons of the rat prefrontal cortex. Cereb Cortex 14:1100-1109.
Schultz W (2015) Neuronal Reward and Decision Signals: From Theories to Data. Physiol Rev 95:853-951.
Serrano-Barroso A, Vargas JP, Diaz E, O'Donnell P, Lopez JC (2019) Sign and goal tracker rats process differently the incentive salience of a conditioned stimulus. PLoS One 14:e0223109.
Sharpe MJ, Killcross S (2015) The prelimbic cortex directs attention toward predictive cues during fear learning. Learn Mem 22:289-293.
Sierra-Mercado D, Padilla-Coreano N, Quirk GJ (2011) Dissociable roles of prelimbic and infralimbic cortices, ventral hippocampus, and basolateral amygdala in the expression and extinction of conditioned fear. Neuropsychopharmacology 36:529-538.
Simon NW, Gilbert RJ, Mayse JD, Bizon JL, Setlow B (2009) Balancing risk and reward: a rat model of risky decision making. Neuropsychopharmacology 34:2208-2217.
Smith KS, Berridge KC, Aldridge JW (2011) Disentangling pleasure from incentive salience and learning signals in brain reward circuitry. Proc Natl Acad Sci U S A 108:E255-264.
Sotres-Bayon F, Sierra-Mercado D, Pardilla-Delgado E, Quirk GJ (2012) Gating of fear in prelimbic cortex by hippocampal and amygdala inputs. Neuron 76:804-812.

1258 St Onge JR, Floresco SB (2009) Dopaminergic modulation of risk-based decision
1259 making. Neuropsychopharmacology 34:681-697.
1260 Stujenske JM, Likhtik E, Topiwala MA, Gordon JA (2014) Fear and safety engage
1261 competing patterns of theta-gamma coupling in the basolateral amygdala.
1262 Neuron 83:919-933.
1263 Sun X, Bernstein MJ, Meng M, Rao S, Sorensen AT, Yao L, Zhang X, Anikeeva PO, Lin
1264 Y (2020) Functionally Distinct Neuronal Ensembles within the Memory Engram.
1265 Cell 181:410-423 e417.
1266 Tan KR, Yvon C, Turiault M, Mirzabekov JJ, Doehner J, Labouebe G, Deisseroth K, Tye
1267 KM, Luscher C (2012) GABA neurons of the VTA drive conditioned place
1268 aversion. Neuron 73:1173-1183.
1269 Tomie A, Aguado AS, Pohorecky LA, Benjamin D (2000) Individual differences in
1270 pavlovian autoshaping of lever pressing in rats predict stress-induced
1271 corticosterone release and mesolimbic levels of monoamines. Pharmacol
1272 Biochem Behav 65:509-517.
1273 Totah NK, Jackson ME, Moghaddam B (2013) Preparatory attention relies on dynamic
1274 interactions between prelimbic cortex and anterior cingulate cortex. Cereb Cortex
1275 23:729-738.
1276 Treanor M, Barry TJ (2017) Treatment of avoidance behavior as an adjunct to exposure
1277 therapy: Insights from modern learning theory. Behav Res Ther 96:30-36.
1278 Tye KM, Prakash R, Kim SY, Fenno LE, Grosenick L, Zarabi H, Thompson KR,
1279 Gradinaru V, Ramakrishnan C, Deisseroth K (2011) Amygdala circuitry mediating
1280 reversible and bidirectional control of anxiety. Nature 471:358-362.
1281 van Zessen R, Phillips JL, Budygin EA, Stuber GD (2012) Activation of VTA GABA
1282 neurons disrupts reward consumption. Neuron 73:1184-1194.
1283 Verharen JPH, van den Heuvel MW, Luijendijk M, Vanderschuren L, Adan RAH (2019)
1284 Corticolimbic Mechanisms of Behavioral Inhibition under Threat of Punishment. J
1285 Neurosci 39:4353-4364.
1286 Vertes RP (2004) Differential projections of the infralimbic and prelimbic cortex in the
1287 rat. Synapse 51:32-58.
1288 Vidal-Gonzalez I, Vidal-Gonzalez B, Rauch SL, Quirk GJ (2006) Microstimulation
1289 reveals opposing influences of prelimbic and infralimbic cortex on the expression
1290 of conditioned fear. Learn Mem 13:728-733.
1291 Vigneswaran G, Kraskov A, Lemon RN (2011) Large identified pyramidal cells in
1292 macaque motor and premotor cortex exhibit "thin spikes": implications for cell
1293 type classification. J Neurosci 31:14235-14242.
1294 Vogel JR, Beer B, Clody DE (1971) A simple and reliable conflict procedure for testing
1295 anti-anxiety agents. Psychopharmacologia 21:1-7.
1296 Volkow ND, Wang GJ, Fowler JS, Tomasi D, Baler R (2012) Food and drug reward:
1297 overlapping circuits in human obesity and addiction. Curr Top Behav Neurosci
1298 11:1-24.
1299 Wakabayashi KT, Feja M, Baindur AN, Bruno MJ, Bhimani RV, Park J, Hausknecht K,
1300 Shen RY, Haj-Dahmane S, Bass CE (2019) Chemogenetic activation of ventral
1301 tegmental area GABA neurons, but not mesoaccumbal GABA terminals, disrupts
1302 responding to reward-predictive cues. Neuropsychopharmacology 44:372-380.

1303 Warthen DM, Lambeth PS, Ottolini M, Shi Y, Barker BS, Gaykema RP, Newmyer BA,
1304 Joy-Gaba J, Ohmura Y, Perez-Reyes E, Guler AD, Patel MK, Scott MM (2016)
1305 Activation of Pyramidal Neurons in Mouse Medial Prefrontal Cortex Enhances
1306 Food-Seeking Behavior While Reducing Impulsivity in the Absence of an Effect
1307 on Food Intake. Front Behav Neurosci 10:63.
1308 Weir K, Blanquie O, Kilb W, Luhmann HJ, Sinning A (2014) Comparison of spike
1309 parameters from optically identified GABAergic and glutamatergic neurons in
1310 sparse cortical cultures. Front Cell Neurosci 8:460.
1311 Widge AS, Heilbronner SR, Hayden BY (2019) Prefrontal cortex and cognitive control:
1312 new insights from human electrophysiology. F1000Res 8.
1313 Zhang X, Kim J, Tonegawa S (2020) Amygdala Reward Neurons Form and Store Fear
1314 Extinction Memory. Neuron 105:1077-1093 e1077.

1315

FIGURE 1

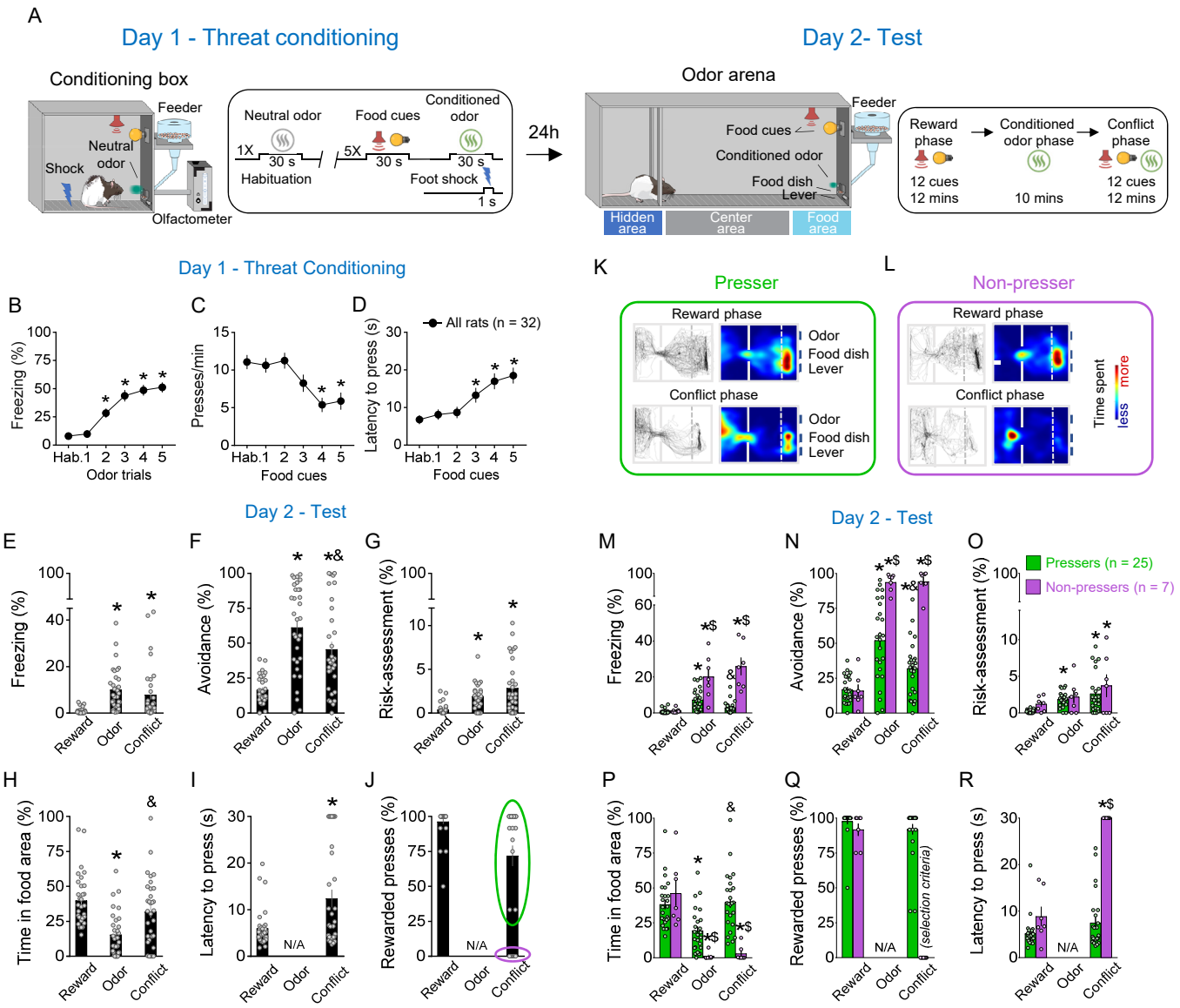
A
Day 1 - Threat conditioning
Conditioning box
Feeder
Neutral odor
Shock
Olfactometer
Neutral odor
Food cues
Conditioned odor
1X
30 s
Habituation
5X
30 s
30 s
Foot shock
1 s
24h
Day 2- Test
Odor arena
Feeder
Food cues
Conditioned odor
Food dish
Lever
Hidden area
Center area
Food area
Reward phase
12 cues
12 mins
Conditioned odor phase
10 mins
Conflict phase
12 cues
12 mins
Day 1 - Threat Conditioning
B
Freezing (%)
Odor trials
C
Presses/min
Food cues
D
Latency to press (s)
All rats (n = 32)
Food cues
K
Presser
Reward phase
Odor
Food dish
Lever
Conflict phase
Odor
Food dish
Lever
L
Non-presser
Reward phase
Conflict phase
Time spent
more
less
Day 2 - Test
E
Freezing (%)
Reward
Odor
Conflict
F
Avoidance (%)
G
Risk-assessment (%)
H
Time in food area (%)
I
Latency to press (s)
N/A
J
Rewarded presses (%)
N/A
Day 2 - Test
M
Freezing (%)
N
Avoidance (%)
O
Risk-assessment (%)
Pressers (n = 25)
Non-pressers (n = 7)
P
Time in food area (%)
Q
Rewarded presses (%)
N/A
(selection criteria)
R
Latency to press (s)
N/A

Figure 1. Rats show individual variability in reward-seeking responses during an approach-avoidance conflict test. (A) Schematic and timeline of the approach-avoidance conflict test. **(B-D)** Rats exhibited an increase in the percentage of time freezing ($F_{(3.117, 96.63)} = 30.4$, $p < 0.0001$) and a reduction in lever presses ($F_{(3.771, 116.9)} = 11.59$, $p < 0.0001$) with a higher latency to press the lever ($F_{(3.29, 102)} = 13.09$, $p < 0.0001$) during the olfactory threat conditioning session on day 1 (n = 32), when compared to before the shock. **(E-G)** Patterns of defensive responses and food seeking during the different phases (reward, odor, conflict) of the test session on day 2. Rats showed an increase in defensive responses characterized by an augment in the percentage of time exhibiting (E) freezing ($F_{(1.678, 52.01)} = 16.56$, $p < 0.0001$), (F) avoidance ($F_{(1.85, 57.36)} = 38.99$, $p < 0.0001$) and (G) risk-assessment ($F_{(1.367, 42.38)} = 17.41$, $p = 0.014$) ; and a decrease in the (H) percentage of time spent in the food area ($F_{(1.63, 50.52)} = 23.81$, $p < 0.0001$) during the odor presentation, when compared to the reward phase. Rats' defensive responses were significantly attenuated during the conflict phase as evidenced by a reduction in the percentage of time (F) avoiding the odor ($p = 0.0031$) and an increase in the percentage of time (H) approaching the food area ($p < 0.0001$) , when compared to the odor phase. **(I-J)** Two different behavioral phenotypes emerged during the conflict phase: rats that continued to press the lever (*Pressers*, green circle, n= 25) and rats that showed a complete suppression in lever pressing (*Non-pressers*, purple circle, n= 7). The % of rewarded presses was calculated as the percentage of the 12 cue trials in which rats pressed the lever. **(K-L)** Representative tracks and heatmaps of time spent in each compartment of the arena for a (K) *Presser* or a (L) Non-Pressers rat during the test session. **(M-R)** Patterns of defensive responses and food seeking during the different phases (reward, odor, conflict) of the test session on day 2 after separating the animals into *Pressers* and *Non-pressers.* When compared to *Non-Pressers, Pressers* showed reduced defensive responses characterized by an attenuation in the percentage of time exhibiting (M) freezing ($F_{(2, 60)} = 29.54$, $p < 0.0001$) and (N) avoidance responses ($F_{(2, 60)} = 23.27$, $p < 0.0001$), and an augment in the percentage of time (P) approaching the food area ($F_{(2, 60)} = 22.49$, $p<0.0001$) during both the odor and the conflict phases. Data shown as mean ± SEM. One-way or two-way ANOVA repeated measures followed by Tukey's or Bonferroni's multiple comparisons tests, all * p's < 0.05 compared to the same group during the reward phase, all & p's < 0.05 compared to the same group during the odor phase, all $ p's < 0.05 compared to *Pressers* during the same phase. All statistical analysis details are presented in table S1. See also Supplementary Fig. 1 and Supplementary Video 1.

FIGURE 2

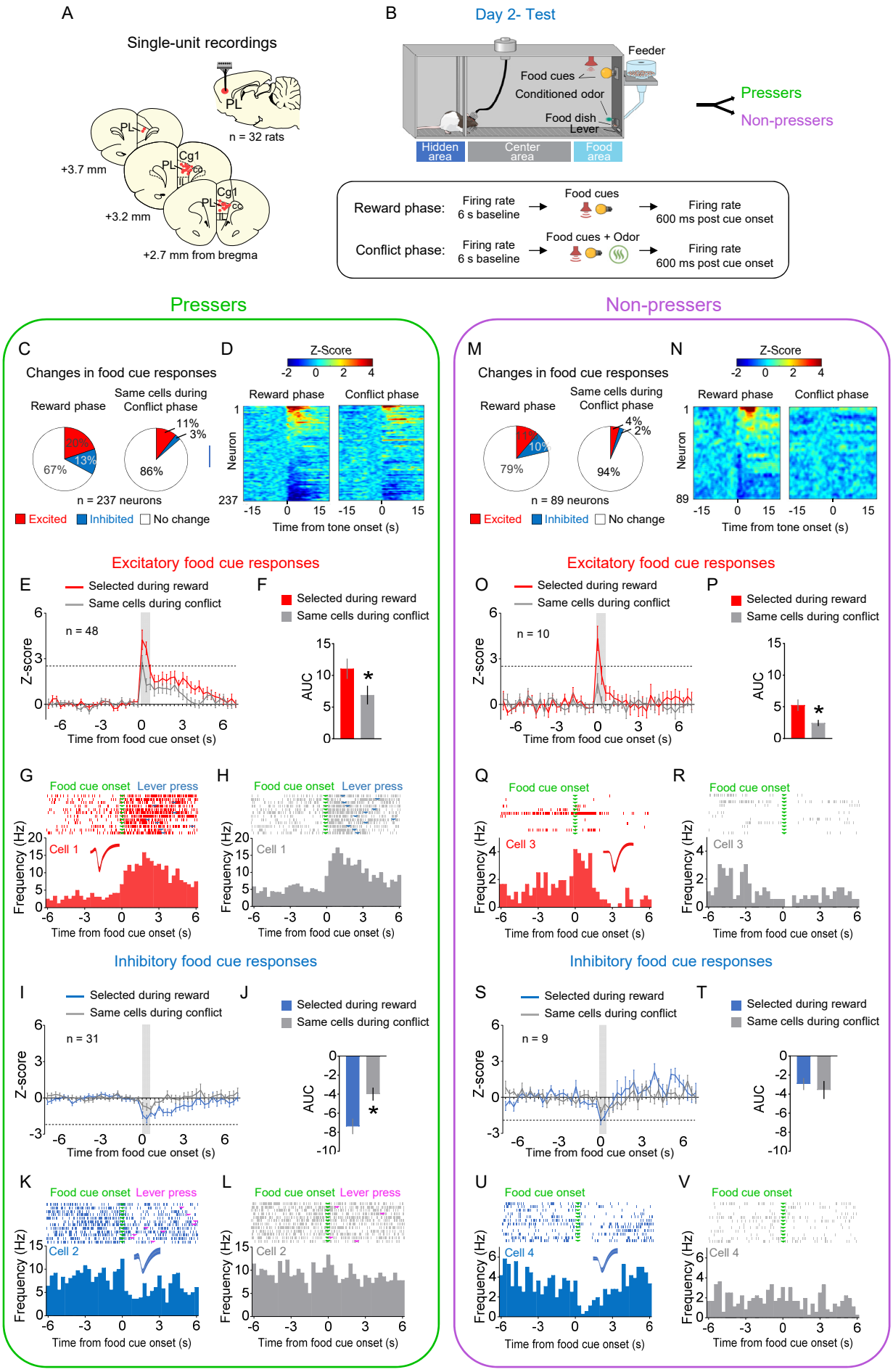
A
Single-unit recordings
PL
n = 32 rats
+3.7 mm
Cg1
+3.2 mm
+2.7 mm from bregma
B
Day 2- Test
Feeder
Food cues
Conditioned odor
Food dish
Lever
Hidden area
Center area
Food area
Pressers
Non-pressers
Reward phase:
Firing rate 6 s baseline
Food cues
Firing rate 600 ms post cue onset
Conflict phase:
Firing rate 6 s baseline
Food cues + Odor
Firing rate 600 ms post cue onset
Pressers
Non-pressers
C
Changes in food cue responses
Reward phase
Same cells during Conflict phase
20%
13%
67%
11%
3%
86%
n = 237 neurons
Excited
Inhibited
No change
D
Z-Score
Reward phase
Conflict phase
Neuron
Time from tone onset (s)
Excitatory food cue responses
E
Selected during reward
Same cells during conflict
n = 48
Z-score
Time from food cue onset (s)
F
AUC
G
Food cue onset
Lever press
Cell 1
Frequency (Hz)
Time from food cue onset (s)
H
Inhibitory food cue responses
I
n = 31
J
K
Cell 2
L
M
Changes in food cue responses
11%
10%
79%
4%
2%
94%
n = 89 neurons
N
O
n = 10
P
Q
Cell 3
R
S
n = 9
T
U
Cell 4
V

Figure 2. PL neurons respond differently to reward cues in *Pressers* vs. *Non-Pressers* during conflict (A) Diagram of the electrode placements in PL. **B)** Schematic and timeline of PL recordings for food cue responses during of the approach-avoidance conflict test (12 food cues per phase). **(C)** Pie charts showing changes in PL firing rate in response to food cues during reward (left) vs. conflict (right) phases for *Pressers* (n = 237 neurons from 25 rats, Fisher's exact test, excitatory during reward phase: n = 48, excitatory during conflict phase: n = 25, p = 0.0049; inhibitory during reward phase: n = 31, inhibitory during conflict phase: n = 7, p < 0.0001. **(D)** Heatmap of Z-scored neural activities for PL neurons selected during reward phase and tracked to conflict phase. **(E)** Average peri-stimulus time histograms (PSTHs) for all PL neurons showing excitatory food cue responses (Z-score > 2.58, dotted line) during reward (red line) compared to the same cells during conflict (gray line). **(F)** Differences in the positive area under the curve (AUC) between the two phases (Wilcoxon test, W = -824, excitatory responses reward phase vs. conflict phase, p < 0.0001). **(G-H)** Representative PSTHs for a PL neuron showing excitatory responses to food cues during the (G) reward phase vs. the same neuron during the (H) conflict phase. **(I)** Average PSTHs for all PL neurons showing inhibitory food cue responses (Z-score < -1.96, dotted line) during reward (blue line) compared to the same cells during conflict (gray line). **(J)** Differences in the negative AUC between the two phases (Wilcoxon test, W = 367, excitatory responses reward phase vs. conflict phase, p < 0.0001). **(K-L)** Representative PSTHs for a PL neuron showing inhibitory responses to food cues during the reward phase (K) vs. the same neuron during the conflict phase (L). **(M)** Pie charts showing changes in PL firing rate in response to food cues during reward (left) vs. conflict (right) phases for *Non-Pressers* (n= 89 neurons from 7 rats; Fisher's exact test, excitatory during reward phase: n = 10, excitatory during conflict phase: n = 4, p = 0.1620; inhibitory during reward phase: n = 9, inhibitory during conflict phase: n = 2, p = 0.0573). **(N-O)** Same as D-E, but for *Non-Pressers*. **(P)** Differences in the positive AUC between the two phases (Wilcoxon test, W = -37, excitatory responses reward phase vs. conflict phase, p = 0.032). **(Q-S)** Same as G-I, but for *Non-Pressers*. **(T)** Differences in the negative AUC between the two phases (Wilcoxon test, W = -3, excitatory responses reward phase vs. conflict phase, p = 0.455). **(U-V)** Same as K-L, but for *Non-Pressers*. Legend: cc, corpus callosum, CG1, anterior cingulate cortex; IL, infralimbic cortex. All statistical analysis details are presented in table S1. See also Supplementary Figs. 2 and 3.

FIGURE 3

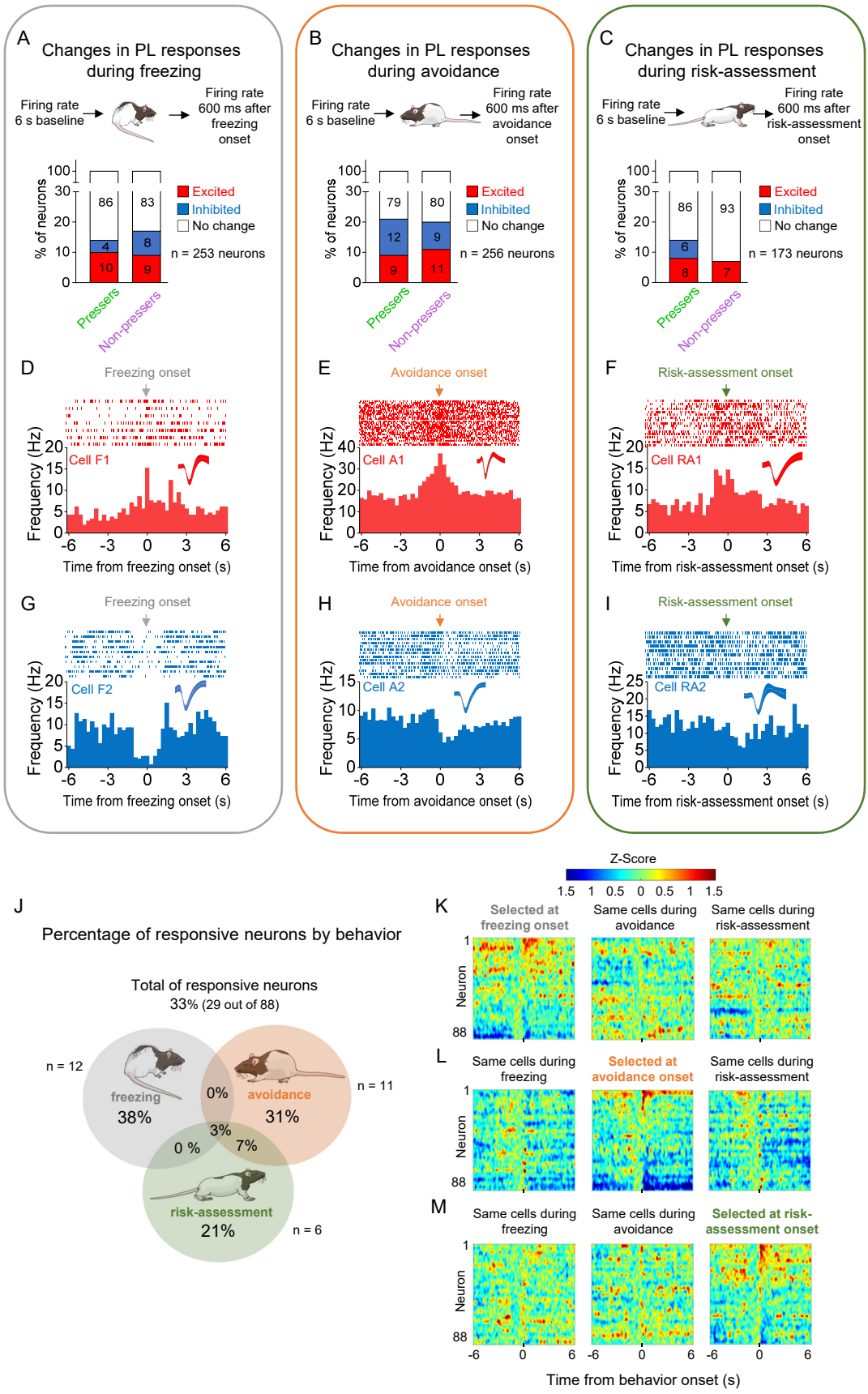
A
Changes in PL responses during freezing
Firing rate 6 s baseline
Firing rate 600 ms after freezing onset
% of neurons
Excited
Inhibited
No change
n = 253 neurons
Pressers
Non-pressers
B
Changes in PL responses during avoidance
Firing rate 6 s baseline
Firing rate 600 ms after avoidance onset
n = 256 neurons
C
Changes in PL responses during risk-assessment
Firing rate 6 s baseline
Firing rate 600 ms after risk-assessment onset
n = 173 neurons
D
Freezing onset
Cell F1
Frequency (Hz)
Time from freezing onset (s)
E
Avoidance onset
Cell A1
Time from avoidance onset (s)
F
Risk-assessment onset
Cell RA1
Time from risk-assessment onset (s)
G
Freezing onset
Cell F2
Time from freezing onset (s)
H
Avoidance onset
Cell A2
Time from avoidance onset (s)
I
Risk-assessment onset
Cell RA2
Time from risk-assessment onset (s)
J
Percentage of responsive neurons by behavior
Total of responsive neurons
33% (29 out of 88)
n = 12
freezing
38%
0%
avoidance
31%
n = 11
3%
0 %
7%
risk-assessment
21%
n = 6
Z-Score
K
Selected at freezing onset
Same cells during avoidance
Same cells during risk-assessment
Neuron
L
Same cells during freezing
Selected at avoidance onset
Same cells during risk-assessment
M
Same cells during freezing
Same cells during avoidance
Selected at risk-assessment onset
Time from behavior onset (s)

Figure 3. PL activity correlates with the onset of freezing, avoidance or risk-assessment behaviors in both *Pressers* and *Non-Pressers*. (A-C) Both *Pressers* and *Non-Pressers* showed the same number and proportion of excitatory and inhibitory PL responses during the onset of (A) freezing (Fisher's exact test, responsive neurons in *Pressers*: 22 neurons, in *Non-Pressers*: 15 neurons, $p = 0.462$), (B) avoidance (Fisher's exact test, responsive neurons in *Pressers*: 43 neurons, in *Non-Pressers*: 9 neurons, $p = 0.999$) or (C) risk-assessment (Fisher's exact test, responsive neurons in *Pressers*: 12 neurons, in *Non-Pressers*: 6 neurons, $p = 0.318$) behaviors. **(D-F)** Representative PSTHs for distinct PL neurons showing excitatory responses at the onset of (D) freezing, (E) avoidance or (F) risk-assessment behaviors. **(G-I)** Representative PSTHs for distinct PL neurons showing inhibitory responses at the onset of freezing (G), avoidance (H) or risk-assessment (I) behaviors. **(J)** Venn Diagram showing the percentage of all PL responsive neurons (29 out of 88 neurons) by behavior. Most of the responsive neurons responded exclusively at the onset of one of the behaviors. **(K-M)** Heatmap of Z-scored neural activities for PL neurons selected at the onset of freezing (K), avoidance (L) or risk-assessment behavior (M) with the same cells tracked during the other behaviors. The threshold used to identify significant differences per neurons was Z-score > 2.58 for excitation and Z-score < -1.96 for inhibition. All statistical analysis details are presented in table S1.

FIGURE 4

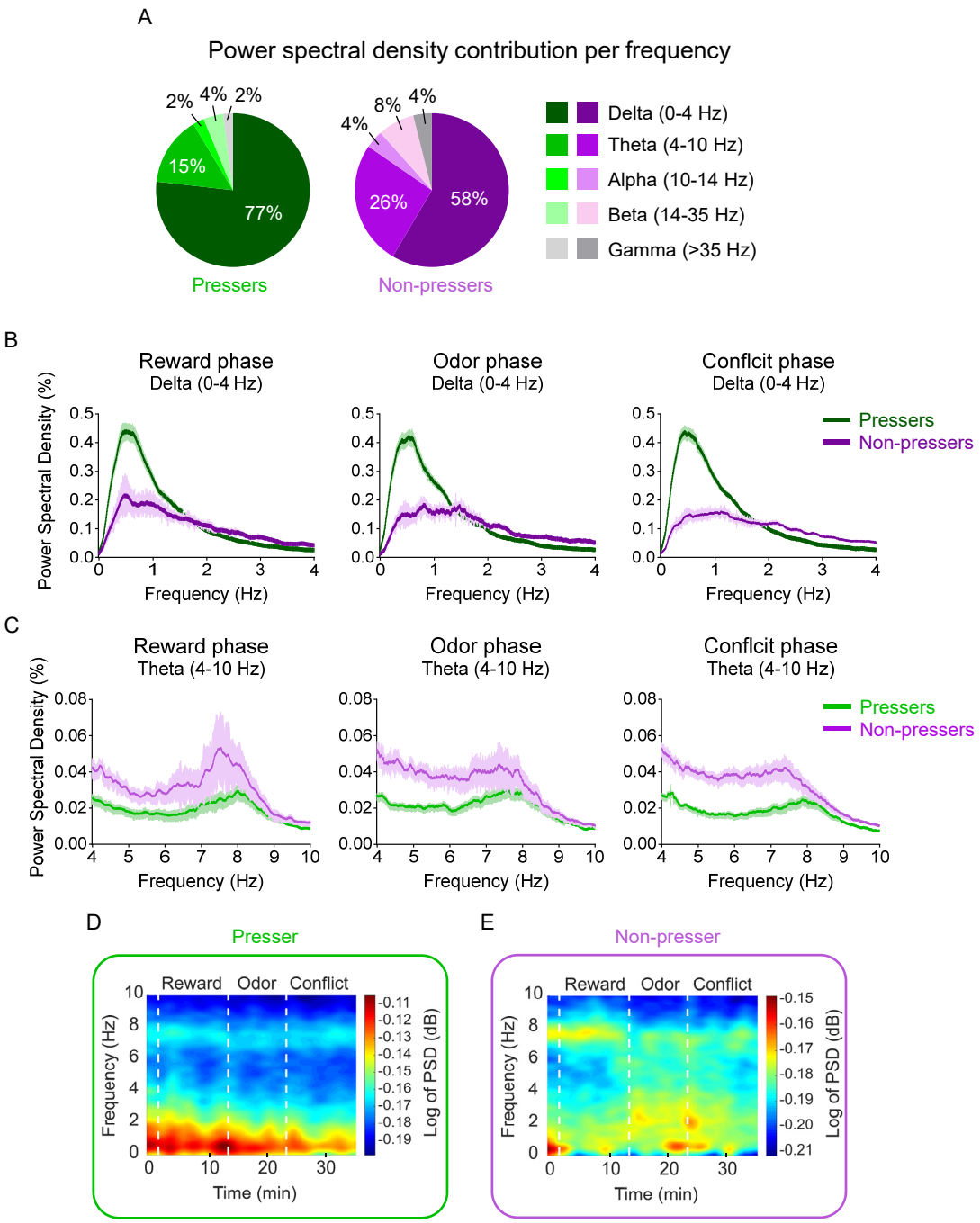
A
Power spectral density contribution per frequency
2%
4%
2%
15%
77%
Pressers
8%
4%
4%
26%
58%
Non-pressers
Delta (0-4 Hz)
Theta (4-10 Hz)
Alpha (10-14 Hz)
Beta (14-35 Hz)
Gamma (>35 Hz)
B
Reward phase
Delta (0-4 Hz)
Odor phase
Delta (0-4 Hz)
Conflcit phase
Delta (0-4 Hz)
Power Spectral Density (%)
Frequency (Hz)
Pressers
Non-pressers
C
Reward phase
Theta (4-10 Hz)
Odor phase
Theta (4-10 Hz)
Conflcit phase
Theta (4-10 Hz)
Power Spectral Density (%)
Frequency (Hz)
Pressers
Non-pressers
D
Presser
Reward
Odor
Conflict
Frequency (Hz)
Time (min)
Log of PSD (dB)
E
Non-presser
Reward
Odor
Conflict
Frequency (Hz)
Time (min)
Log of PSD (dB)

Figure 4. *Pressers* and *Non-Pressers* show significant differences in PL oscillations during the test session. (A) Power spectral density (PSD) contribution at different frequency bands. **(B-C)** Average of PSD (%) in the (B) delta (0-4 Hz) or (C) theta (4-10 Hz) bands in *Pressers* (green line, n = 25 rats) and *Non-Pressers* (purple line, n = 7 rats) during the (left) reward, (center) odor, and (right) conflict phases of the test session. *Pressers* showed increased power in the delta band, whereas *Non-Pressers* showed increased power in the theta band during the three phases of the test session (Unpaired Student's t-test comparing *Pressers* vs. *Non-Pressers*, All p's < 0.0001) . **(D-E)** Representative time-frequency spectrogram showing changes in the log of PSD (dB) for delta and theta bands in (D) *Pressers* and (E) *Non-Pressers* across the different phases of the session. All statistical analysis details are presented in table S1.

FIGURE 5

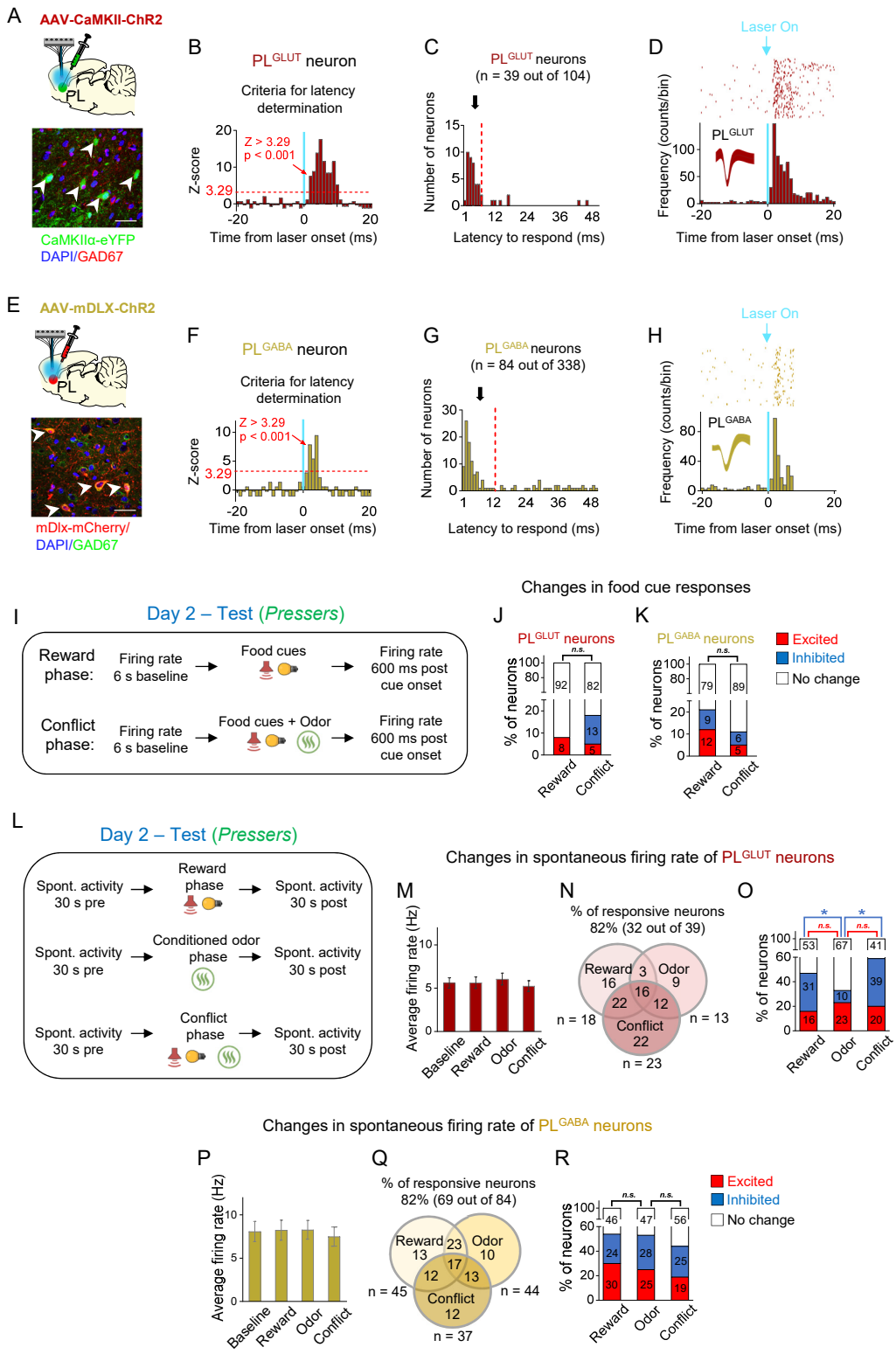
A
AAV-CaMKII-ChR2
PL
CaMKIIα-eYFP
DAPI/GAD67
B
PL^GLUT neuron
Criteria for latency determination
Z > 3.29
p < 0.001
3.29
Z-score
Time from laser onset (ms)
C
PL^GLUT neurons
(n = 39 out of 104)
Number of neurons
Latency to respond (ms)
D
Laser On
PL^GLUT
Frequency (counts/bin)
Time from laser onset (ms)
E
AAV-mDLX-ChR2
PL
mDlx-mCherry/
DAPI/GAD67
F
PL^GABA neuron
Criteria for latency determination
Z > 3.29
p < 0.001
3.29
Z-score
Time from laser onset (ms)
G
PL^GABA neurons
(n = 84 out of 338)
Number of neurons
Latency to respond (ms)
H
Laser On
PL^GABA
Frequency (counts/bin)
Time from laser onset (ms)
I
Day 2 – Test (Pressers)
Reward phase:
Firing rate 6 s baseline
Food cues
Firing rate 600 ms post cue onset
Conflict phase:
Firing rate 6 s baseline
Food cues + Odor
Firing rate 600 ms post cue onset
Changes in food cue responses
J
PL^GLUT neurons
% of neurons
Reward
Conflict
K
PL^GABA neurons
Excited
Inhibited
No change
L
Day 2 – Test (Pressers)
Spont. activity 30 s pre
Reward phase
Spont. activity 30 s post
Conditioned odor phase
Conflict phase
Changes in spontaneous firing rate of PL^GLUT neurons
M
Average firing rate (Hz)
Baseline
Reward
Odor
Conflict
N
% of responsive neurons
82% (32 out of 39)
Reward 16
Odor 9
Conflict 22
n = 18
n = 13
n = 23
O
% of neurons
Reward
Odor
Conflict
Changes in spontaneous firing rate of PL^GABA neurons
P
Average firing rate (Hz)
Baseline
Reward
Odor
Conflict
Q
% of responsive neurons
82% (69 out of 84)
Reward 13
Odor 10
Conflict 12
n = 45
n = 44
n = 37
R
Excited
Inhibited
No change
% of neurons
Reward
Odor
Conflict

Figure 5. In pressers, PL^{GLUT} neurons show reduced spontaneous activity during the conflict phase. (A) Top, Schematic of viral infusion. Bottom, Representative immunohistochemical micrograph showing lack of colabeling (white arrows) between the ChR2 viral construct (green, AAV-CaMKII-ChR2-eYFP) and the GABA marker GAD67 (red), confirming that the use of a CaMKII promoter enables transgene expression favoring PL glutamatergic neurons. Scale bars: 25 µm. **(B-D)** Photoidentification of PL^{GLUT} neurons. (B) Frequency histogram showing the latency of response to laser illumination for PL neurons (n = 39 photoidentified PL^{GLUT} neurons out of 104 recorded cells). (C) Cells with photoresponse latencies < 6 ms were classified as PL^{GLUT} neurons (Z-score > 3.29, $p < 0.001$, red dotted line, see details in Methods). (D) Raster plot and peristimulus time histogram showing a representative PL^{GLUT} neuron responding to a 5 Hz train of laser stimulation. **(E)** Top, Schematic of viral infusion. Bottom, Representative immunohistochemical micrograph showing colabeling (white arrows) between the ChR2 viral construct (red, AAV-mDlx-ChR2-mCherry) and the GABA marker GAD67 (green), confirming that the use of a mDlx promoter enables transgene expression favoring PL GABA neurons. Scale bars: 25 µm. **(F-H)** Photoidentification of PL^{GABA} neurons. (F) Frequency histogram showing the latency of response to laser illumination for PL neurons (n = 84 photoidentified PL^{GABA} neurons out of 338 recorded neurons). (G) Cells with photoresponse latencies < 12 ms were classified as PL^{GABA} neurons (Z-score > 3.29, $p < 0.001$, red dotted line, see details in Methods). (H) Raster plot and peristimulus time histogram showing a representative PL^{GABA} neuron responding to a 5Hz train of laser stimulation. Vertical blue bars: laser onset. Bins of 1 ms. **(I)** Timeline of PL recordings for food cue responses in *Pressers* during test (12 food cues per phase). **(J-K)** Stacked bar showing the percentage of (J) PL^{GLUT} neurons or (K) PL^{GABA} neurons that changed their firing rates in response to food cues from the reward phase to the conflict phase. No significant differences were observed across the phases (Fisher's exact test, all p's > 0.05; n.s. = non-significant). **(L)** Timeline of PL recordings for spontaneous activity in *Pressers* during test. **(M)** Average firing rate of PL^{GLUT} neurons across the different phases of test. **(N)** Venn diagram showing the percentage of responsive PL^{GLUT} neurons (32 out of 39 neurons) by events. **(O)** Stacked bar showing the percentage of PL^{GLUT} neurons that changed their spontaneous firing rates across the different phases of the test. PL^{GLUT} neurons were disinhibited during the odor phase (Fisher's exact test, inhibited in Reward phase: 12 neurons, inhibited in Odor phase: 4 neurons, $p = 0.047$) and subsequently inhibited during the conflict phase (Fisher's exact test, inhibited in Odor phase: 4 neurons, inhibited in Conflict phase: 15 neurons, $p = 0.0073$). **(P)** Average firing rate of PL^{GABA} neurons across the different phases of test. **(Q)** Venn diagram showing the percentage of responsive PL^{GABA} neurons (69 out of 84 neurons) by events. **(R)** Stacked bar showing the percentage of PL^{GABA} neurons that changed their spontaneous firing rates across the different phases of the test. No significant differences were observed across the phases (Fisher's exact test, all p's > 0.05; n.s. = non-significant). All statistical analysis details are presented in table S1. See also Supplementary Figs. 4, 5, 6 and 7.

FIGURE 6

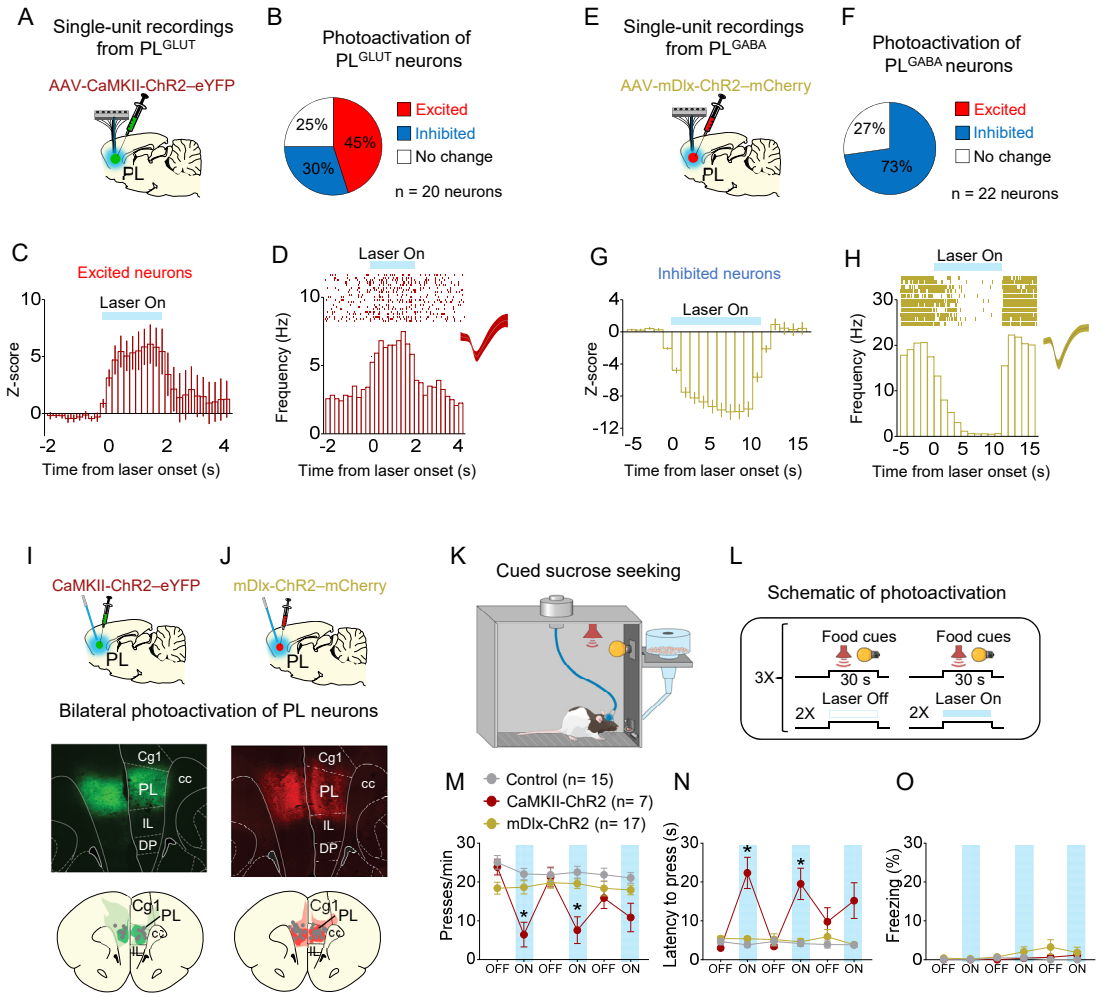
A
Single-unit recordings from PL^GLUT
AAV-CaMKII-ChR2–eYFP
PL
B
Photoactivation of PL^GLUT neurons
25%
45%
30%
Excited
Inhibited
No change
n = 20 neurons
E
Single-unit recordings from PL^GABA
AAV-mDlx-ChR2–mCherry
PL
F
Photoactivation of PL^GABA neurons
27%
73%
Excited
Inhibited
No change
n = 22 neurons
C
Excited neurons
Laser On
Z-score
Time from laser onset (s)
D
Laser On
Frequency (Hz)
Time from laser onset (s)
G
Inhibited neurons
Laser On
Z-score
Time from laser onset (s)
H
Laser On
Frequency (Hz)
Time from laser onset (s)
I
CaMKII-ChR2–eYFP
PL
J
mDlx-ChR2–mCherry
PL
Bilateral photoactivation of PL neurons
Cg1
PL
cc
IL
DP
K
Cued sucrose seeking
L
Schematic of photoactivation
Food cues
Food cues
3X
30 s
30 s
Laser Off
Laser On
2X
2X
M
Control (n= 15)
CaMKII-ChR2 (n= 7)
mDlx-ChR2 (n= 17)
Presses/min
OFF ON OFF ON OFF ON
N
Latency to press (s)
OFF ON OFF ON OFF ON
O
Freezing (%)
OFF ON OFF ON OFF ON

Figure 6. Photoactivation of PL^{GLUT}, but not PL^{GABA}, neurons suppresses reward seeking in a neutral context. (A) Schematic of viral infusion and recordings in PL. **(B)** Changes in PL firing rate with illumination of PL^{GLUT} neurons in rats expressing AAV-CaMKII-ChR2-eYFP in PL (n= 20 neurons). **(C)** Average PSTH of PL neurons that were excited during laser illumination of PL^{GLUT} neurons. **(D)** Raster plot and peri-stimulus time histogram (PSTH) of representative PL neuron showing excitatory responses to illumination in rats expressing AAV-CaMKII-ChR2-eYFP in PL. **(E)** Schematic of viral infusion and recordings in PL. **(F)** Changes in PL firing rate with illumination of PL^{GABA} neurons in rats expressing AAV-mDlx-ChR2-mCherry in PL (n= 22 neurons). **(G)** Average PSTH of PL neurons that were inhibited during laser illumination of PL^{GABA} neurons. **(H)** Raster plot and PSTH of representative PL neuron showing inhibitory responses to illumination in rats expressing AAV-mDlx-ChR2-mCherry in PL. **(I-J)** Representative micrograph showing the expression of (I) CaMKII-ChR2-eYFP or (J) mDlx-ChR2-mChery in PL and schematic of optical fiber location (gray dots) in the same region (compressed across different antero-posterior levels of PL). Green or red areas represent the minimum (dark) and the maximum (light) viral expression into the PL. **(K-L)** Schematic and timeline of PL photostimulation during the cued-sucrose seeking test in a neutral context. **(M-N)** Optogenetic activation of PL^{GLUT} neurons (CaMKII-ChR2, dark red circles, n= 7), but not PL^{GABA} neurons (mDlx-ChR2, gold circles, n= 17), reduced the (M) frequency of bar presses ($F_{(10, 180)} = 7.009$, $p<0.0001$, CaMKII-ChR2 OFF vs ON Tukey post hoc, $p < 0.0001$) and increased (N) the latency for the first press ($F_{(10, 180)} = 9.931$, $p < 0.0001$, CaMKII-ChR2 OFF vs ON Tukey post hoc, $p < 0.0001$) when compared to the control group (eYFP-control virus, gray circles, n = 15). **(O)** Optogenetic activation of PL neurons did not alter freezing behavior ($F_{(10, 180)} = 1.124$, $p = 0.3463$). Blue shaded area represents laser-on trials (PL^{GLUT}: 5 Hz, PL^{GABA}: 20 Hz; 5ms pulse width,7-10 mW, 30 s duration). Data shown as mean ± SEM. Each circle represents the average of two consecutive trials. Two-way repeated-measures ANOVA followed by Bonferroni post hoc test. All * p's < 0.05. All statistical analysis details are presented in table S1.

FIGURE 7

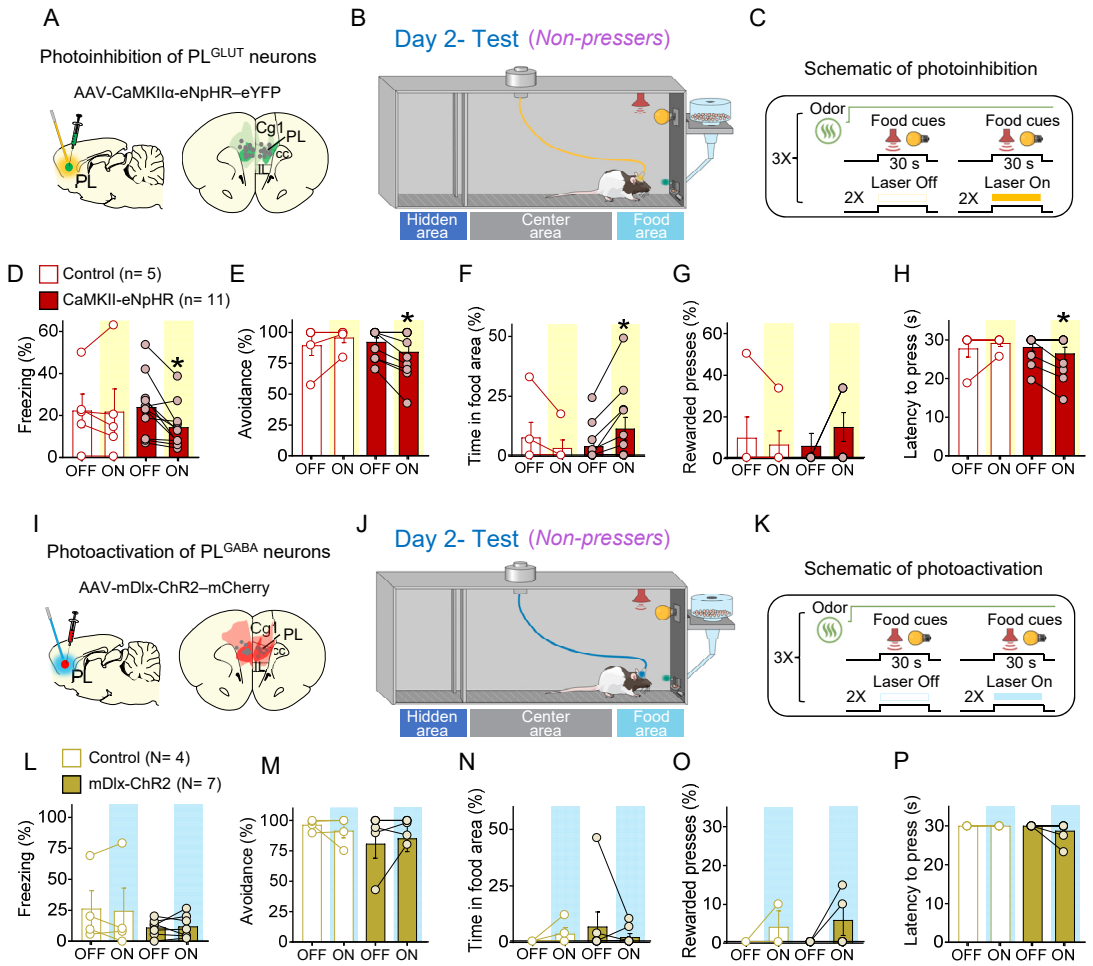
A
Photoinhibition of PL^GLUT neurons
AAV-CaMKIIα-eNpHR–eYFP
PL
Cg1
PL
IL
CC
B
Day 2- Test (Non-pressers)
Hidden area
Center area
Food area
C
Schematic of photoinhibition
Odor
Food cues
Food cues
3X
30 s
30 s
Laser Off
Laser On
2X
2X
D
Control (n= 5)
CaMKII-eNpHR (n= 11)
Freezing (%)
E
Avoidance (%)
F
Time in food area (%)
G
Rewarded presses (%)
H
Latency to press (s)
OFF ON OFF ON
I
Photoactivation of PL^GABA neurons
AAV-mDlx-ChR2–mCherry
J
Day 2- Test (Non-pressers)
K
Schematic of photoactivation
L
Control (N= 4)
mDlx-ChR2 (N= 7)
M
N
O
P

Figure 7. Photoinhibition of PL^{GLUT} neurons during conflict reduces freezing and increases food approaching in *Non-Pressers*. (A) Schematic of AAV-CaMKII-eNpHR–eYFP virus infusion in PL and location of optical fibers (gray dots) in the same region (compressed across different antero-posterior levels of PL). Green areas represent the minimum (dark) and the maximum (light) viral expression into the PL. **(B-C)** Schematic and timeline of the approach-avoidance conflict test during optogenetic inactivation of PL^{GLUT} neurons. **(D-H)** Photoinhibition of PL^{GLUT} neurons (CaMKII-eNpHR, red bars, n = 11) during the conflict test reduced the percentage of time rats spent (D) freezing (Wilcoxon test, W = -64, laser OFF vs. laser ON, p = 0.0020) and (E) avoiding the odor area (Wilcoxon test, W = -21, laser OFF vs. laser ON, p = 0.031) , and increased the percentage of time rats spent in the (F) food area (Wilcoxon test, W = -31, laser OFF vs. laser ON, p = 0.031) during the conflict test without altering (G) the number of lever presses (Wilcoxon test, W = 6, laser OFF vs. laser ON, p = 0.250) and (H) the latency to press (Wilcoxon test, W = -10, laser OFF vs. laser ON, p = 0.125), when compared to controls (eYFP-control virus, white bars, n= 5, Wilcoxon test, Freezing: W = 3, p = 0.812, avoidance: W = 3, p = 0.500, food area: W = 3, p = 0.500, lever presses: W = -1, p = 0.999, latency to press: W = 1, p = 0.999). **(I)** Schematic of AAV-mDlx-ChR2–mCherry virus infusion in PL and location of optical fibers (gray dots) in the same region (compressed across different antero-posterior levels of PL). Red areas represent the minimum (dark) and the maximum (light) viral expression into the PL **(J-K)** Schematic and timeline of the approach-avoidance conflict test during optogenetic activation of PL^{GABA} neurons. **(L-P)** Photoactivation of PL^{GABA} neurons during the conflict test did not alter rats' behavior (mDlx-ChR2, gold bars, n= 7, Wilcoxon test, Freezing: W = 18, p = 0.156, avoidance: W = 4, p = 0.500, food area: W = -2, p = 0.750, lever presses: W = 3, p = 0.500, latency to press: W = -3, p = 0.500), when compared to controls (eYFP-control virus, white bars, n = 4, Wilcoxon test, Freezing: W = -2, p = 0.875, avoidance: W = 0, p = 0.999, food area: W = 3, p = 0.500, lever presses: W = 1, p = 0.500, latency to press: all animals reached maximum latency). PL neurons were illuminated from cue onset until the animals pressed the bar or from cue onset until the end of the 30s cues if the animals didn't press the bar (PL^{GLUT}: 5 Hz, PL^{GABA}: 20 Hz; 5ms pulse width,7-10 mW). Data shown as mean ± SEM. Each bar represents the average of six trials alternated in blocks of 2. Note that the number of data points may appear fewer than the number of rats per group because multiple animals showed the same values. Two-way ANOVA repeated measures followed by Bonferroni post hoc test. All * p's < 0.05. All statistical analysis details are presented in table S1. See also Supplementary Fig 8.

FIGURE 8

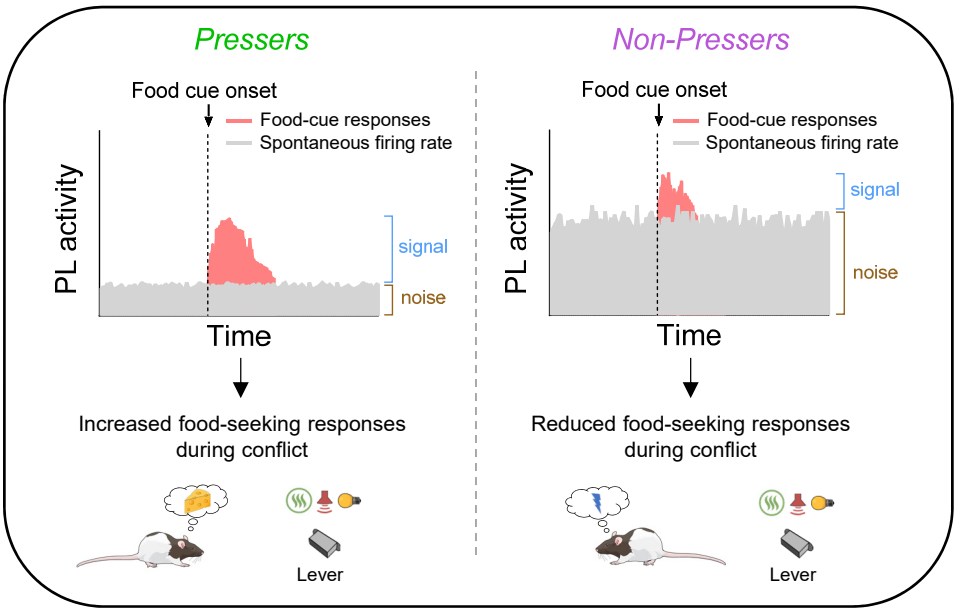
Pressers
Food cue onset
Food-cue responses
Spontaneous firing rate
PL activity
signal
noise
Time
Increased food-seeking responses during conflict
Lever
Non-Pressers
Food cue onset
Food-cue responses
Spontaneous firing rate
PL activity
signal
noise
Time
Reduced food-seeking responses during conflict
Lever

Figure 8. Schematic showing differences in food-cue responses and spontaneous firing rate of PL neurons in *Pressers* and *Non-Pressers.* Left, *Pressers* showed reduced spontaneous firing rate and increased food-cue responses in PL neurons during the conflict test, which resulted in higher signal-to-noise ratio and increased food-seeking responses. Right, *Non-Pressers* showed increased spontaneous firing rate and reduced food-cue responses in PL neurons during the conflict test, which resulted in lower signal-to-noise ratio and reduced food-seeking responses.